

**AD-A281 299**



OFFICE OF NAVAL RESEARCH

CONTRACT N00014-89-J-1828

R&T Code 3132080

Abstract Report #4

**DTIC**  
**ELECTE**  
**JUL 11 1994**  
**S F D**

TOWARDS TOBACCO MOSAIC VIRUS-LIKE SELF-ASSEMBLED SUPRAMOLECULAR  
ARCHITECTURES

by

V. Percec, J. Heck, G. Johansson and D. Tomazos

Published

in the

Macromol. Symp., 77, 237 (1994)

Department of Macromolecular Science  
Case Western Reserve University  
Cleveland, OH 44106-7202

June 30, 1994

DTIC QUALITY INSPECTED 2

Reproduction in whole or in part is permitted for any purpose of the United States Government

This document has been approved for public release and sale;  
its distribution is unlimited.

**94-20939**



**BEST  
AVAILABLE COPY**

**94 7 8 040**

## REPORT DOCUMENTATION PAGE

FORM 100-104-1188  
OMB No. 104-0188

1. This report is the property of the Government and is loaned to your agency; it and its contents are not to be distributed outside your agency without prior approval of the Office of Management and Budget. Send comments regarding this burden estimate or any other aspect of this collection of information, including suggestions for reducing this burden, to Washington Headquarters Services, Directorate for Information Operations and Reports, 1215 Jefferson Davis Highway, Suite 1204, Arlington, VA 22202-4302, and to the Office of Management and Budget, Paperwork Reduction Project (10704-0188), Washington, DC 20503.

|  |   |  |   |  |
|--|---|--|---|--|
| 1. AGENCY USE ONLY (Leave blank)   |   | 2. REPORT DATE<br>June 30, 1994                            | 3. REPORT TYPE AND DATES COVERED<br>Abstract Report #4                  |  |
| 4. TITLE AND SUBTITLE<br>Towards Tobacco Mosaic Virus-like Self-Assembled Supramolecular Architectures   |   |  | 5. FUNDING NUMBERS<br>N00014-89-J-1828                                  |  |
| 6. AUTHOR(S)<br>V. Percec, J. Heck, G. Johansson and D. Tomazos  |   |  |   |  |
| 7. PERFORMING ORGANIZATION NAME(S) AND ADDRESS(ES)<br>Department of Macromolecular Science<br>Case Western Reserve University<br>Cleveland, OH 44106-7202  |   |  | 8. PERFORMING ORGANIZATION<br>REPORT NUMBER<br>N00014-89-J-1828         |  |
| 9. SPONSORING/MONITORING AGENCY NAME(S) AND ADDRESS(ES)<br>Department of Navy<br>Office of Naval Research<br>800 North Quincy Street<br>Arlington, VA 22217-5000   |   |  | 10. SPONSORING/MONITORING<br>AGENCY REPORT NUMBER<br>Abstract Report #4 |  |
| 11. SUPPLEMENTARY NOTES<br>Macromolecular Symposia, <u>77</u> , 237 (1994)   |   |  |   |  |
| 12a. DISTRIBUTION/AVAILABILITY STATEMENT   |   |  | 12b. DISTRIBUTION CODE  |  |
| 13. ABSTRACT (Maximum 200 words)<br><p>This paper discusses the molecular design of selected examples of structural units containing taper shaped <i>exo</i>-receptors and various crown ether, oligooxyethylenic, and H-bonding based <i>endo</i>-receptors, which self-assemble into cylindrical channel-like architectures <i>via</i> principles resembling those of tobacco mosaic virus (TMV). The ability of these structural units to self-assemble <i>via</i> a delicate combination of <i>exo</i>- and <i>endo</i>-recognition processes will be presented. A comparison between various <i>supramolecular</i> (generated <i>via</i> H-bonding, ionic, and electrostatic interactions) and <i>molecular</i> "polymer backbones" will be made. The present limitations concerning the ability to engineer the structural parameters of these supramolecular channel-like architectures and some possible novel material functions derived from them will be briefly mentioned.</p> |   |  |   |  |
| 14. SUBJECT TERMS  |   |  | 15. NUMBER OF PAGES   |  |
|  |   |  | 16. PRICE CODE  |  |
| 17. SECURITY CLASSIFICATION<br>OF REPORT<br>Unclassified   | 18. SECURITY CLASSIFICATION<br>OF THIS PAGE<br>Unclassified | 19. SECURITY CLASSIFICATION<br>OF ABSTRACT<br>Unclassified | 20. LIMITATION OF ABSTRACT<br>U1  |  |

# TOWARDS TOBACCO MOSAIC VIRUS-LIKE SELF-ASSEMBLED SUPRAMOLECULAR ARCHITECTURES

V. Percec\*, J. Heck, G. Johansson, and D. Tomazos

Department of Macromolecular Science, Case Western Reserve University,  
Cleveland, OH 44106, USA

G. Ungar

Department of Engineering Materials and Centre for Molecular Materials, The  
University of Sheffield, Sheffield, S1 1DU, UK

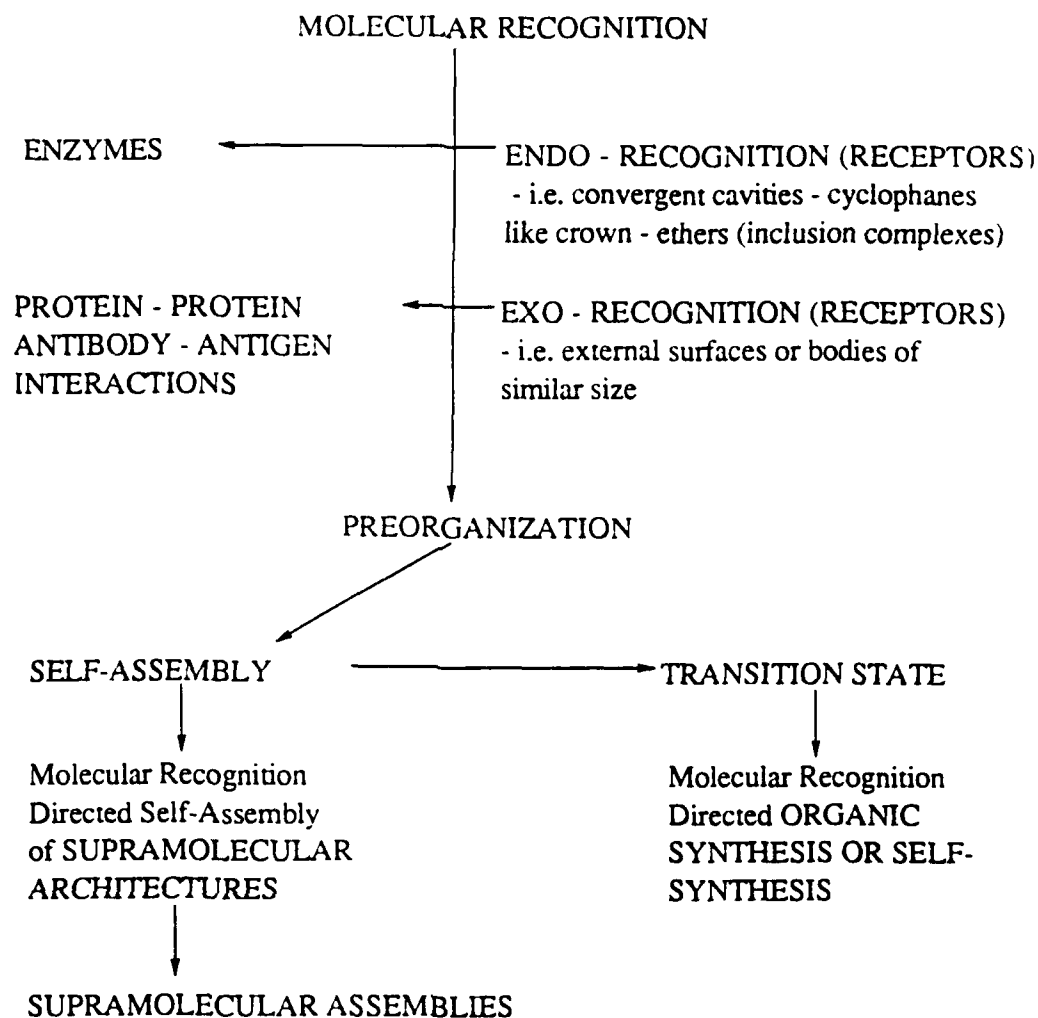
**Abstract:** This paper discusses the molecular design of selected examples of structural units containing taper shaped *exo*-receptors and various crown ether, oligoetherethylenic, and H-bonding based *endo*-receptors, which self-assemble into cylindrical channel-like architectures *via* principles resembling those of tobacco mosaic virus (TMV). The ability of these structural units to self-assemble *via* a delicate combination of *exo*- and *endo*-recognition processes will be presented. A comparison between various *supramolecular* (generated *via* H-bonding, ionic, and electrostatic interactions) and *molecular* "polymer backbones" will be made. The present limitations concerning the ability to engineer the structural parameters of these supramolecular channel-like architectures and some possible novel material functions derived from them will be briefly mentioned.

## INTRODUCTION

For the past 150 years organic chemists were concerned mainly with the understanding of the covalent bond. Recently, research on molecular recognition (generated by weak, non-covalent interactions) has been recognized worldwide as an important intellectual and technological frontier.<sup>1</sup> *Endo*- (generated by convergent cavities) and *exo*- (generated by larger bodies of similar size and shapes, or surfaces) molecular recognition,<sup>2</sup> preorganization, and self-organization provide the basis of spontaneous generation of functional supramolecular architectures *via* self-assembly from their components (Scheme 1).<sup>3</sup> Molecular recognition directed organic synthesis or self-synthesis,<sup>4</sup> and self-assembly of supramolecular architectures<sup>2,3</sup> are two of the most active topics of supramolecular chemistry.<sup>2a</sup> It is well accepted that molecular recognition directed synthesis and self-assembly are responsible for the generation and the fascinating properties of biological systems. Tobacco mosaic virus (TMV) represents the best understood self-assembled biological system.<sup>2a,b,5</sup> Therefore, we believe it provides an ideal model to be used for the understanding of the principles governing the self-assembly of synthetic supramolecular architectures.

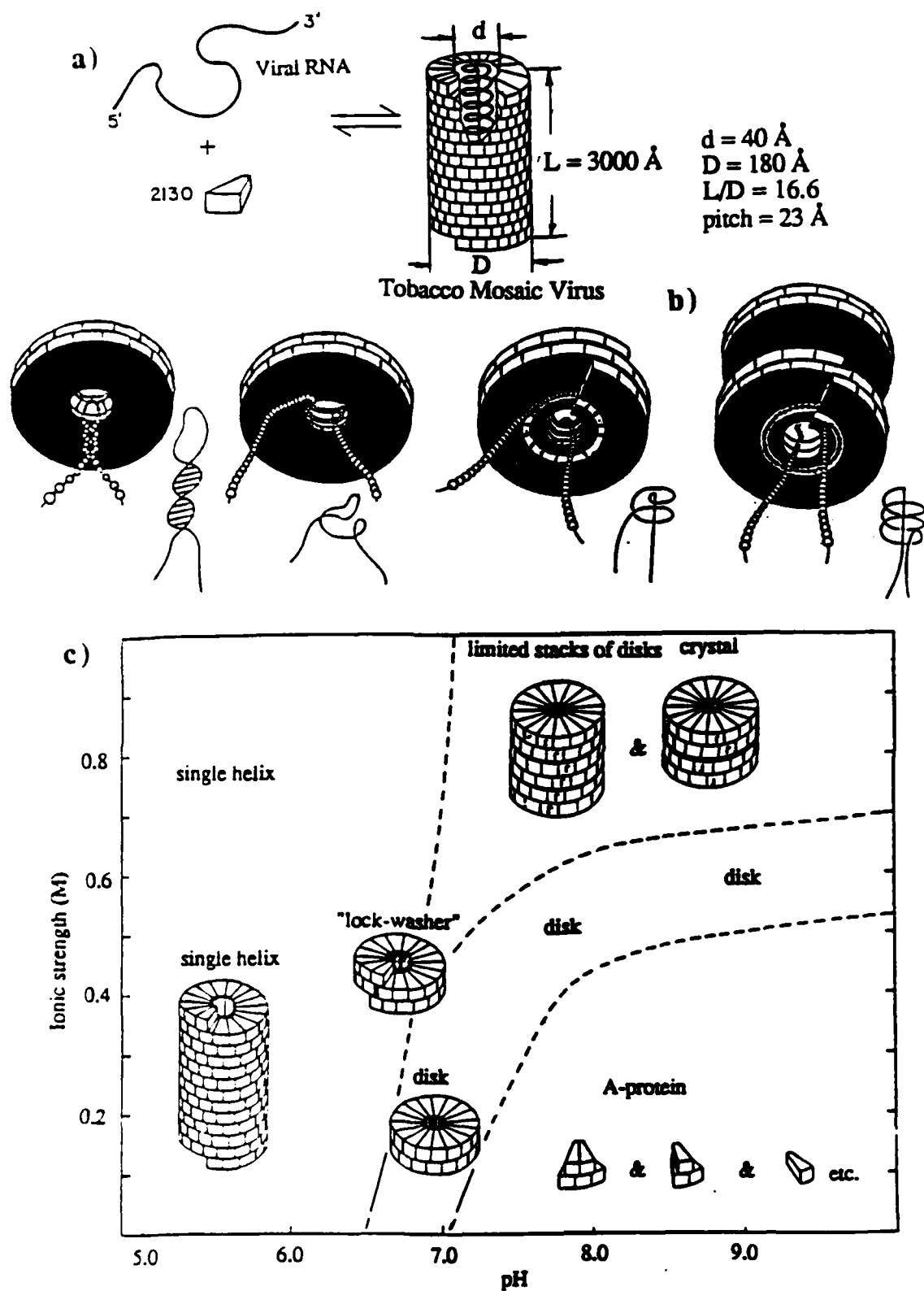
## SYNTHETIC STRATEGY USED IN THE DESIGN OF TMV-LIKE SUPRAMOLECULAR ARCHITECTURES

TMV is a simple virus consisting only of a single type of protein molecule and of a transcribed nucleic acid (RNA), the carrier of genetic information. Figure 1 provides a

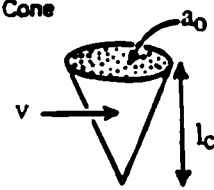
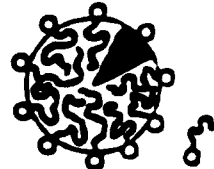

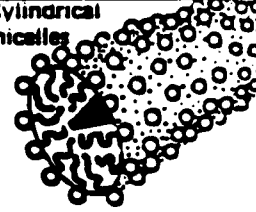

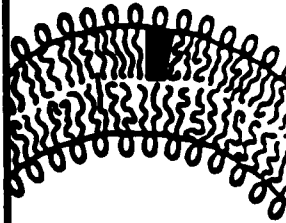

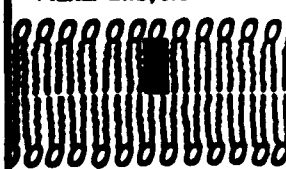

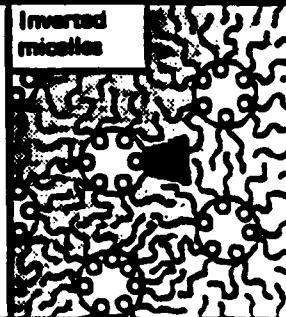


Scheme 1: Supramolecular chemistry pathways

simplified picture of its self-assembly. Its single rod-shape results from its design, namely a regular helical array of 2130 identical protein molecules (or subunits) in which is embedded a single molecule of RNA. The virus dimensions are 3000 Å in length, 180 Å in diameter, a helical pitch of 23 Å, and a central hole of 40 Å. TMV self-assembles upon mixing of its individual components. Therefore, it is considered that all the information necessary to assemble TMV is contained in its components, i.e. mostly within the protein subunits. Under certain pH conditions the proteins self-assemble into a TMV even in the absence of RNA. Therefore, either RNA or pH can initiate the conformational change of a double or single layered disc from its disc-like shape into a lock-washer shape which is responsible for the generation of the single helix of TMV. The first driving force towards this self-assembled system is provided by the *exo*-recognition of the tapered shapes of the proteins. *Exo*-recognition makes use of an external surface and the *exo*-receptor substrate binding occurs by surface to surface interaction.<sup>2a</sup> Therefore, *exo*-recognition with strong selective binding requires a large enough contact area and a sufficient number of interactions as well as



**Figure 1:** The assembly of the Tobacco Mosaic Virus: (a) from its constituent protein subunits and viral RNA into a cylindrically shaped tubular supramolecule; (b) the threading of the RNA in a hairpin conformation into a double layered disc of protein subunits initiating the change to a lock-washer conformation; (c) the dependence of the self-assembly of the protein subunits on pH (adapted from ref. 3a, 5, and 10).

| Lipid   | Critical packing parameter $v/a_0 l_c$ | Critical packing shape  | Structures formed   |
|---|--|---|---|
| Single-chained lipids with large head group areas               | $< 1/3$                                | Cone<br>                                | Spherical micelles<br>           |
| Single-chained lipids with small head group areas               | $1/3-1/2$                              | Truncated cone<br>                      | Cylindrical micelles<br>         |
| Double-chained lipids with large head-group areas, fluid chains | $1/2-1$                                | Truncated cone<br>                     | Flexible bilayers, vesicles<br> |
| Double-chained lipids with small head-group areas               | $\sim 1$                               | Cylinder<br>                         | Planar bilayers<br>            |
| Double-chained lipids with small head-group areas               | $> 1$                                  | Inverted truncated cone or wedge<br> | Inverted micelles<br>          |

**Figure 2:** The dependence of the shape of lipids on the structures which they self-assemble into:  $a_0$ =optimal head group area;  $l_c$ =critical chain length;  $v$ =volume of hydrocarbon chains (adapted from reference 6).

geometrical and site complementarity between the two surfaces. Consequently, *exo*-recognition includes recognition between large bodies of similar size as well as recognition at interfaces. Protein-protein and antibody-antigen interactions occur *via* an *exo*-recognition process while enzymes function *via* an *endo*-recognition process.<sup>2a</sup> Consequently, the first step towards a TMV-like self-assembly consists of the design of synthetic organic molecules having a specific tapered shape which resembles that of the proteins from Figure 1. Lipids are classic molecules whose shape is determined by the number of chains and the ratio between their head and tail diameters.<sup>6</sup> In addition, they self-assemble into spherical and cylindrical micelles and bilayer structures whose architectures are determined by the shape of the lipid (Figure 2). The shape of the lipid can be manipulated *via* temperature and the amount of water of hydration. At higher concentrations, cylindrical micelles self-assemble into a hexagonal columnar mesophase, spherical micelles self-assemble into a cubic mesophase, while layered structures assemble into lamellar mesophases.<sup>7</sup> Therefore, at a different scale, the self-assembly of the cylindrical micelles of lipids resembles the self-assembly of the constituent proteins of TMV. The simplest non-amphiphilic homologue of lipids with a tapered shape can be designed by the alkylation of alkyl 3,4,5-trihydroxybenzoate with either bromoalkanes or with alkoxybenzyloxybenzyl chloride. Variants of these taper shaped side groups were attached to polymer backbones either *via* polymer homologues<sup>8</sup> or by polymerization<sup>9,10</sup> reactions. The resulting polymers self-assemble into cylindrical architectures which generate a columnar hexagonal ( $\Phi_h$ ) liquid crystalline phase. These preliminary experiments have demonstrated that various substituted gallic acid derivatives can be used to construct *exo*-receptors with a tapered shape.

This paper will review some of our efforts directed towards the molecular design of TMV-like supramolecular architectures *via* synthetic strategies consisting of various combinations of molecular and supramolecular chemistries.

## SUPRAMOLECULAR CYLINDERS BY A COMBINATION OF *ENDO*- AND *EXO*-RECOGNITION.

### Crown Ethers as *Endo*-Receptors

Crown ethers are a class of *endo*-receptors containing an endohydrophilic cavity ideally suited for the binding of positively charged substrates. The binding ability of crown ethers is controlled by a number of factors including the size of the macrocycle, the number of donor atoms present in the cycle, its conformational flexibility, and the electronic effects of substituents present on the macrocycle. We have demonstrated that by taking all these factors into consideration, it is possible to design highly selective *endo*-receptors based on crown ethers that can ultimately facilitate the self-assembly of various supramolecular architectures.

For the present study, two crown ether *endo*-receptors have been employed. Their synthesis has been reported previously,<sup>11,12</sup> and is outlined in Figure 3. In the first case, the conformationally rigid 4-hydroxymethyl(benzo-15-crown-5) (**B15C5**) *endo*-receptor was employed. In the second case, the more conformationally flexible ( $\pm$ )-hydroxymethyl(15-





crown-5) (**15C5**) *endo*-receptor was used. No thermodynamic data for complexes of **15C5** and **B15C5** with sodium cations under comparable conditions are available in the literature. However, the stability constants ( $\log K_S$ ), where  $K_S = k_{\text{complexation}}/k_{\text{decomplexation}}$  ( $k_{\text{complexation}}$  and  $k_{\text{decomplexation}}$  are the rate constants for complexation and decomplexation, respectively), can be determined from solution ionic conductivity. Correspondingly,  $\log K_S$  for complexation of **15C5** ( $\log K_S = 2.70$ )<sup>13</sup> and benzo-15-crown-5 ( $\log K_S = 2.68$ )<sup>14</sup> with sodium cations in 90% aqueous MeOH solution, where conformational effects are minimized, are nearly identical. Therefore, any differences in the phase behavior of self-assembled complexes derived from structural units containing **15C5** and **B15C5** *endo*-receptors should result from differences in the conformational flexibility of the two macrocycles and not from differences in their electronic nature.

The facile esterification of **B15C5** or **15C5** with 3,4,5-tris(*p*-dodecyloxybenzyloxy)benzoic acid (**12-ABG**) resulted in the taper shaped structural units, **12-ABG-B15C5** and **12-ABG-15C5**, respectively, which contain one of the two crown ethers as *endo*-receptors and **12-ABG** as the *exo*-receptor (Figure 3). The esterification of **15C5** with 3,4,5-tris(*p*-dodecyloxy)benzoic acid (**12-AG**) yielded a shorter taper shaped structural unit, **12-AG-15C5**, which lacks the benzyl ether moieties in the alkyl tails of its *exo*-receptor. The phase behavior of **12-ABG-B15C5**, **12-ABG-15C5**, and **12-AG-15C5** and of their complexes with sodium triflate (NaOTf) and potassium triflate (KOTf) was investigated by a combination of techniques consisting of differential scanning calorimetry (DSC), thermal optical polarized microscopy, and small (SAXS) and wide angle x-ray scattering (WAXS) and was already discussed in detail.<sup>8-11</sup>

The structure of **12-ABG-B15C5** is shown in Figure 4a. Figure 4b and 4c presents the DSC thermograms from the second heating scan of the complexes of **12-ABG-15C5** with NaOTf and KOTf, respectively. For further elucidation, the dependence of the transition temperatures of **12-ABG-B15C5** and its complexes with NaOTf and KOTf determined by DSC during the first cooling scans are plotted in Figure 4d.

The uncomplexed tapered structural unit, **12-ABG-B15C5**, is crystalline and melts into an isotropic liquid at 96 °C. Its crystalline phase obtained after fresh recrystallization from solution or melt displays a number of sharp small and wide angle reflections corresponding to a lamellar crystalline structure. Complexation of **12-ABG-B15C5** with less than 0.3 moles of NaOTf per **B15C5** decreases its crystallization ability. However, complexation of **12-ABG-B15C5** with as little as 0.4 moles NaOTf per mole **B15C5** results in spontaneous self-assembly of a hexagonal columnar ( $\Phi_h$ ) mesophase at a temperature,  $T > T_g$  ( $T_g$ =glass transition temperature). The presence of a  $T_g$  on the DSC trace of this complex suggests a cooperative motion which is characteristic for polymer systems. Focal conic or fan-shaped textures, which are representative of  $\Phi_h$  mesophases, were observed by optical polarized microscopy. Increasing the amount of NaOTf results in an increase in the isotropic- $\Phi_h$  transition temperature ( $T_i\text{-}\Phi_h$ ). The complex of **12-ABG-B15C5** with as much as 1.8 moles NaOTf per mole of **12-ABG-B15C5** exhibited a  $\Phi_h$

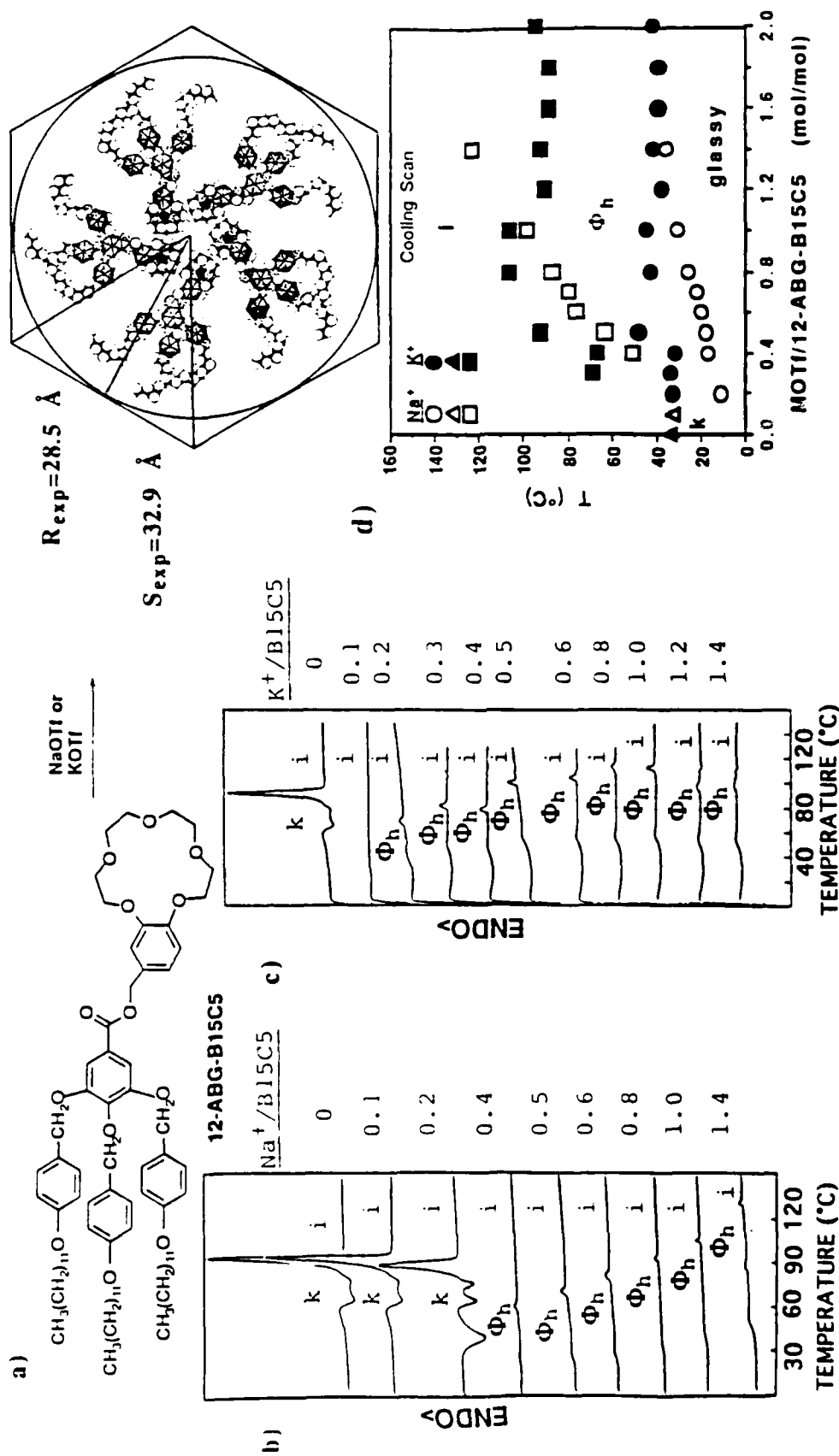


Figure 4: Schematic representation of a cross-section of the supramolecular column formed upon complexation of 12-ABG-B15C5 with sodium triflate (NaOTf) or potassium triflate (KOTf) (a); representative DSC traces (second heating scans, 20 °C/min) of the complexes of 12-ABG-B15C5 with NaOTf (b) and with KOTf (c); the dependence of the transition temperatures of the complexes of 12-ABG-B15C5 with MOTf on the MOTf/12-ABG-B15C5 molar ratio determined during the first DSC cooling scans; M=Na: ○, Tg; △, T<sub>c</sub>; Φ<sub>h</sub>; M=K: ●, Tg; ▲, T<sub>c</sub>; Φ<sub>h</sub> (d).

mesophase. However, at this concentration of NaOTf, the sample was subject to Lewis acid catalyzed decomposition by NaOTf at temperatures higher than 120 °C.

Complexation of **12-ABG-B15C5** with as little as 0.1 moles KOTf per mole of **B15C5** (Figure 4c) results in a glassy compound while its complexation with 0.2 moles of KOTf results in the spontaneous self-assembly of a  $\Phi_h$  mesophase. For comparison, in the case of the complexes of **12-ABG-B15C5** with NaOTf, the formation of a  $\Phi_h$  mesophase required 0.4 moles of salt. This shows that a salt based on a larger cation induces the formation of a  $\Phi_h$  mesophase in **12-ABG-B15C5** at lower concentrations. Furthermore, complexes of **12-ABG-B15C5** with KOTf are characterized by higher isotropization temperatures, and therefore provide a  $\Phi_h$  mesophase with a higher thermal stability than the corresponding complexes with NaOTf.

The primary difference between the complexes of benzo-15-crown-5 with sodium and potassium salts consists in their stability constants and their stoichiometry. Benzo-15-crown-5 forms complexes in solution with both sodium and potassium cations.<sup>15,16</sup> The stability constants of these complexes decrease with increasing cation size. In the solid state, benzo-15-crown-5 forms 1:1 complexes with sodium cations and 2:1 complexes with potassium salts.<sup>16</sup> No information is available for the stoichiometry of these complexes in the liquid crystalline phase. However, we can speculate that their behavior should follow the same general trend observed in the crystalline phase. Sodium prefers to be hexa-coordinated within the crown cavity but benzo-15-crown-5 provides only five coordination sites. Therefore, the sixth coordination site is available for interaction with the counteranion or with a neighboring receptor. Potassium, which prefers to be hepta- or hexa-coordinated, is too large to fit within the crown ether cavity and is, therefore, complexed in a sandwich manner by two moles of benzo-15-crown-5. Consequently, less potassium salt is required to suppress the crystallization of **12-ABG-B15C5** and to generate a  $\Phi_h$  mesophase.

Upon complexation of **12-ABG-B15C5** with more than 1.0 moles of KOTf per mole of **12-ABG-B15C5**,  $T_{i-\Phi_h}$  decreases slightly and then remains nearly constant (Figure 4d). On the other hand,  $T_{i-\Phi_h}$  of the complexes of **12-ABG-B15C5** with more than 1.0 moles of NaOTf per mole of **12-ABG-B15C5** continues to increase up to a molar ratio of 2.0. Transition temperatures of these complexes were not observed by DSC during the cooling scan at salt concentrations greater than 1.4 due to thermal decomposition of the sample during the first heating scan. However, characteristic fan-shaped textures were observed by thermal optical polarized microscopy prior to decomposition at NaOTf/**12-ABG-B15C5** molar ratios greater than 1.4. Since benzo-15-crown-5 forms 1:1 complexes with sodium cations, it is unexpected that more than a 1:1 molar ratio of NaOTf : crown ether in this system results in further stabilization of the mesophase. It is possible that the crown ether behaves both as a selective *endo*-receptor and as a non-selective solvent-like *endo*-receptor in the liquid crystalline phase. Therefore, **12-ABG-B15C5** may dissolve larger amounts of salt than expected based on the behavior of benzo-15-crown-5 in solution and in crystalline phases.

The complex of **12-ABG-B15C5** with 0.6 mol of NaOTf (**12-ABG-B15C5-0.6**) was characterized in the crystalline and  $\Phi_h$  mesophase by SAXS and WAXS experiments. The poorly developed crystalline phase, which can be observed only during the first heating scan or after subsequent annealing, shows numerous weak reflections indicative of a lamellar crystalline structure. In the  $\Phi_h$  mesophase, three reflections with d spacings in the ratio  $d_{100}^{\text{hex}} : d_{110}^{\text{hex}} : d_{200}^{\text{hex}} = 1 : 1/\sqrt{3} : 1/2$ , characteristic of the  $\Phi_h$  mesophase were observed. The radius of the cylindrical column ( $R_{\text{exp}} = a/2$ ) and the side length of the hexagonal column ( $S_{\text{exp}} = 2R/\sqrt{3}$ ) were determined from the hexagonal lattice parameter ( $a = 2d_{100}^{\text{hex}}/\sqrt{3}$ ) to be 28.5 Å and 32.9 Å, respectively.

In order to derive conclusions about the molecular arrangement of **12-ABG-B15C5** within the self-assembled supramolecular columns, molecular models were constructed based on the conformation of related compounds as determined by crystallographic analyses.<sup>11</sup> A possible molecular arrangement is shown in Figure 4a in which the crown ether moieties are arranged side by side within the center of the column layer. The aromatic moieties form a rigid inner core surrounding the melted crown ether *endo*-receptors. The melted alkyl tails of the *exo*-receptor radiate toward the column periphery and may fill the empty space within their own column or interdigitate into the empty space of adjacent columns. The experimentally determined density of the supramolecular structure obtained by complexation indicates that five or six tapered units reside within the column center. The crown ether *endo*-receptors may be stacked on top of each other forming five or six continuous channel-like structures down the column axis. Ionic interactions between complexed and uncomplexed crown ether structural units provide the driving force for this layer-column transformation.

The structure of the taper shaped structural unit, **12-ABG-15C5**, derived from the more conformationally flexible **15C5** *endo*-receptor unit is shown in Figure 5a. The dependence of the transition temperatures of **12-ABG-15C5** and its complexes with NaOTf determined by DSC during the first cooling scan are plotted in Figure 5b. The dependence of the transition temperatures of **12-AG-15C5** and its complexes with NaOTf determined by DSC during the first cooling scan are plotted in the same figure for comparison.

Compound **12-ABG-15C5** is also crystalline and melts into an isotropic liquid at 60 °C. This melting temperature is 36 °C lower than that observed for **12-ABG-B15C5**. Complexation with as little as 0.2 moles NaOTf per mole **12-ABG-15C5** results in the formation of a monotropic  $\Phi_h$  mesophase. As the amount of NaOTf is increased to 0.5 moles, the  $\Phi_h$  mesophase becomes enantiotropic. In the same manner as **12-ABG-B15C5**, increasing the amount of NaOTf suppresses crystallization and increases  $T_{i-\Phi_h}$ . A  $\Phi_h$  mesophase was observed by optical polarized microscopy for complexes of **12-ABG-15C5** with as much as 2.0 moles of NaOTf. Higher concentrations were not investigated. Compound **12-ABG-15C5** displayed a lower  $T_{i-\Phi_h}$  than **12-ABG-B15C5** over the entire composition range. This difference varied between 10 and 20 °C.

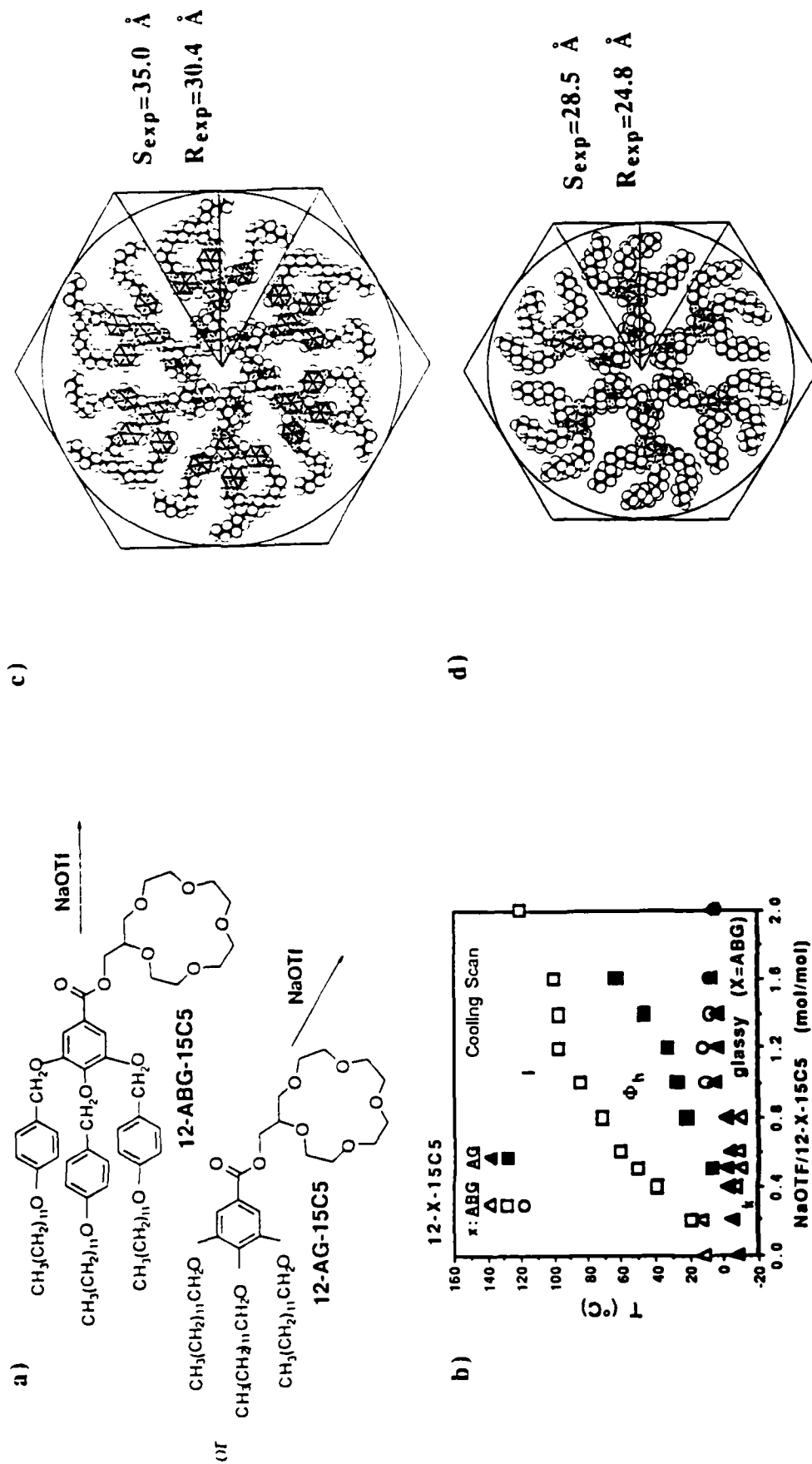


Figure 5: Schematic representation of the complexation of 12-X-15C5 (X=ABG, AG) with sodium triflate (NaOTf) (a); the dependence of the phase transition temperatures of the complexes of 12-X-15C5 (X=ABG: O, T<sub>g</sub>; Δ, T<sub>i-k</sub>; □, T<sub>i-φh</sub>; and X=AG: ▲, T<sub>i-k</sub>; ■, T<sub>i-φh</sub>) (data from the first DSC cooling scans) (b); schematic representation of a cross-section of the supramolecular column formed upon complexation of 12-ABG-15C5 (c) and of 12-AG-15C5 (d) with NaOTf.

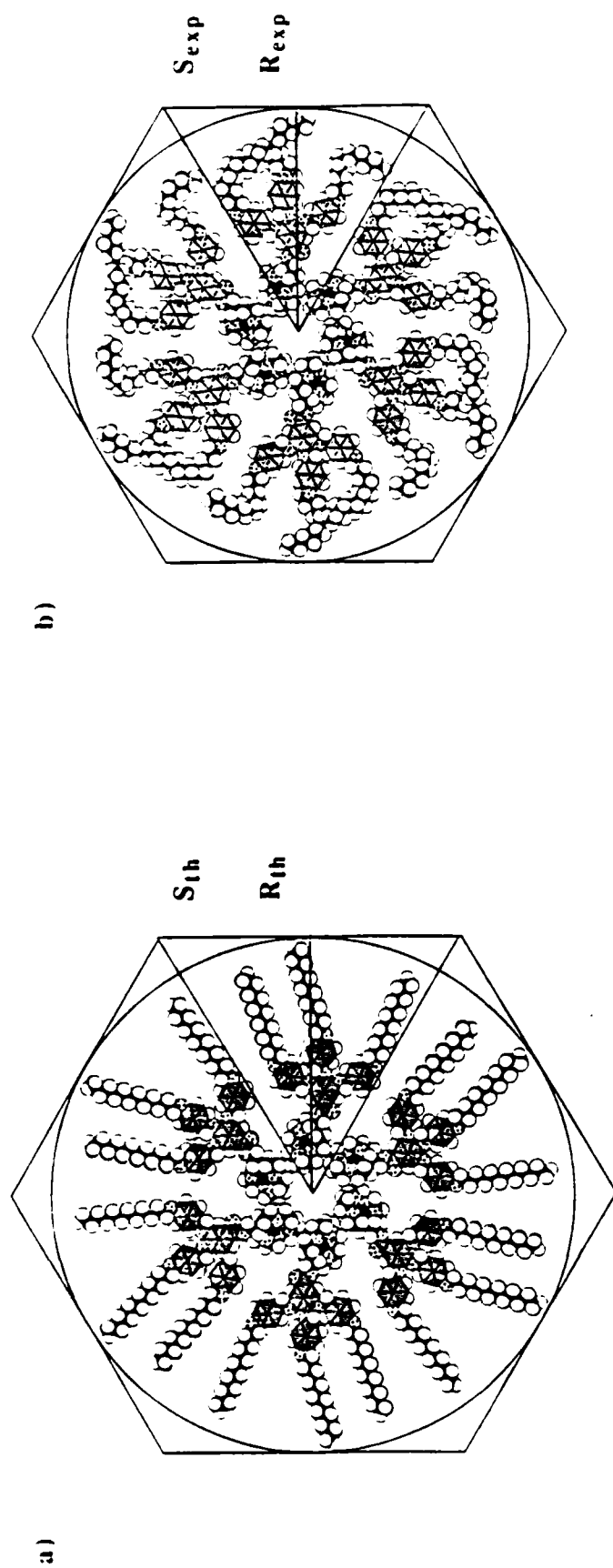
The phase behavior of the complex of **12-ABG-15C5** with 1.6 moles of NaOTf was characterized by SAXS and WAXS experiments. The crystalline phase displays numerous comparatively sharp reflections extending to wide angles. The first four reflections index on a hexagonal lattice. This is in contrast to the lamellar structure observed in the crystalline phase of complexes of **12-ABG-B15C5**. The observed hexagonal packing in **12-ABG-15C5** is most probably a consequence of the increased conformational flexibility of the **15C5** moiety. This flexibility results in fewer conformational restrictions upon complexation and may lead to faster and eventually stronger complexation with alkali metal cations which in turn results in increased interactions between complexed and uncomplexed crown ether structural units within the column center. The role of preorganization of the conformationally flexible *endo*-receptor is a well established event in molecular recognition processes.<sup>17</sup>

In the  $\Phi_h$  mesophase, **12-ABG-15C5** displays the three reflections characteristic of the  $\Phi_h$  mesophase. An arrangement similar to that described for the  $\Phi_h$  mesophase of **12-ABG-B15C5** is depicted in Figure 5c.  $R_{exp}$  and  $S_{exp}$  were determined to be 30.4 Å and 35.0 Å, respectively. For reasons that will be discussed later in this section, it is most probable that six molecules of **12-ABG-15C5** reside within the column center. This quantity is within the limits imposed by the experimentally determined density of the complex. In all other respects, the  $\Phi_h$  mesophase of **12-ABG-15C5** is structurally similar to that described for **12-ABG-B15C5**.

Figure 5a shows the structure of **12-AG-15C5**. This tapered unit is structurally similar to **12-ABG-15C5**. However, the benzyl ether moieties are absent in the alkyl tails of the **12-AG-15C5** *exo*-receptor. The taper shaped *exo*-receptors derived from n-alkyloxy tails are synthetically more accessible and thermochemically more stable than their n-alkyloxybenzyloxy counterparts. The dependence of the transition temperatures of **12-AG-15C5** and its complexes with NaOTf determined by DSC during the first cooling scans are plotted in Figure 5b.

Compound **12-AG-15C5** is crystalline and melts into an isotropic liquid at 32 °C. The complexes of **12-AG-15C5** with NaOTf are crystalline over the entire composition range (0-2.0 mol/mol) but exhibit a monotropic  $\Phi_h$  mesophase at NaOTf / **12-AG-15C5** molar ratios of 0.5 and greater. The  $T_{i-\Phi_h}$  is 50-60 °C lower than the corresponding transitions in **12-ABG-15C5**. Furthermore, a  $T_g$  is not observed due to crystallization during the cooling scan. The kinetically controlled crystallization process is faster for the *exo*-receptor of **12-AG-15C5** than that of **12-ABG-15C5** due to the absence of the benzyl ether moieties.

The phase behavior of the complex of **12-AG-15C5** with 1.6 moles NaOTf was also characterized by WAXS and SAXS experiments. The crystalline phase is a double layer structure with the crown ethers arranged head-to-head within the layers. This is in contrast to the hexagonal order observed in the crystalline phase of **12-ABG-15C5**. In the  $\Phi_h$  mesophase of **12-AG-15C5**, only two reflections were observed at low angles. The fact that the corresponding spacings are in the 2:1 ratio is indicative of a  $\Phi_h$  mesophase. The  $R_{exp}$



| Compound     | No. of Molecules | R <sub>th</sub><br>(Å) | R <sub>exp</sub><br>(Å) | S <sub>exp</sub><br>(Å) | Shrinkage<br>(%) |
|--------------|------------------|------------------------|-------------------------|-------------------------|------------------|
| 12-ABG-B15C5 | 5                | 40.8                   | 28.5                    | 32.9                    | 67               |
| 12-ABG-15C5  | 6                | 41.2                   | 30.4                    | 35.0                    | 57               |
| 12-AG-15C5   | 6                | 34.5                   | 24.8                    | 27.7                    | 59               |

**Figure 6:** Schematic representation of a cross-section of the column generated by the complexation of 12-ABG-15C5 with 1.6 moles of sodium triflate (NaOTf): (a) top view containing six molecules of 12-ABG-15C5 with the alkyl tails extended; (b) top view containing six molecules of 12-ABG-15C5 with the alkyl tails melted to match R<sub>exp</sub>. Similar data for 12-ABG-B15C5 and 12-AG-15C5 are presented in the Table. The theoretical radius (R<sub>th</sub>) for the minimum energy conformation was determined from molecular models.

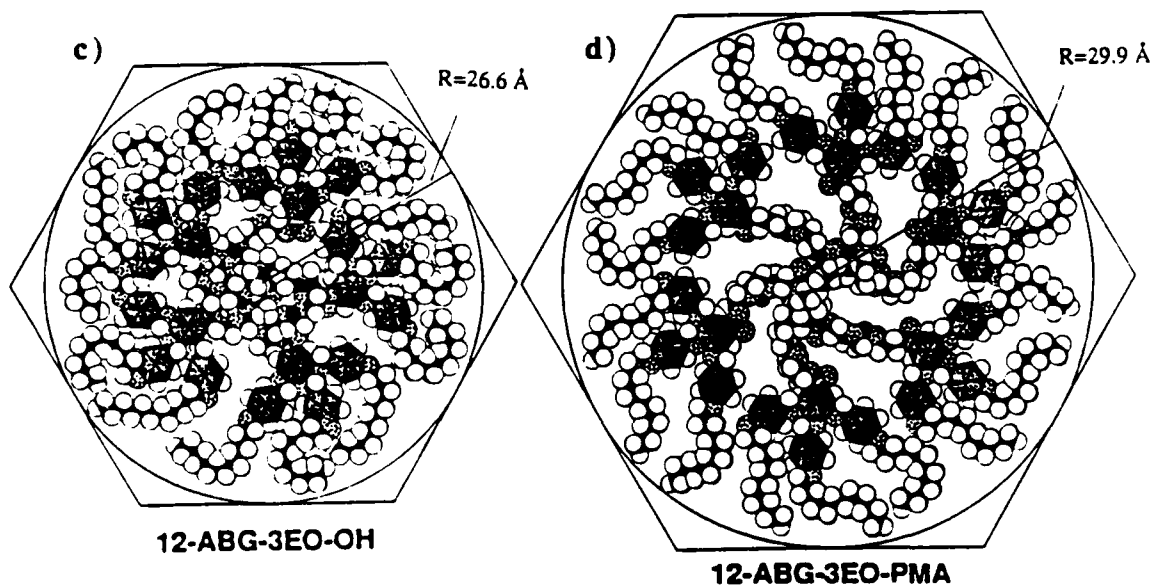
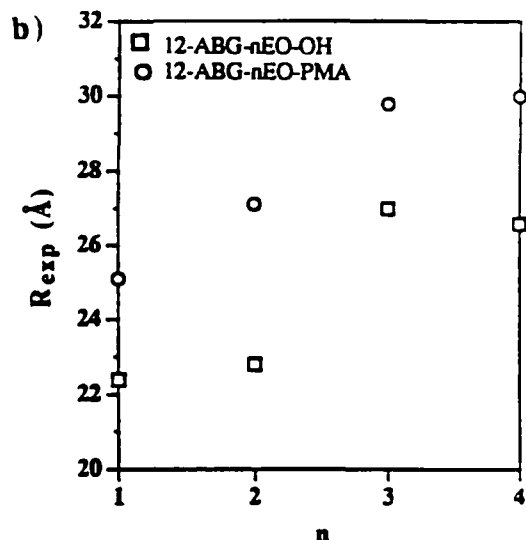
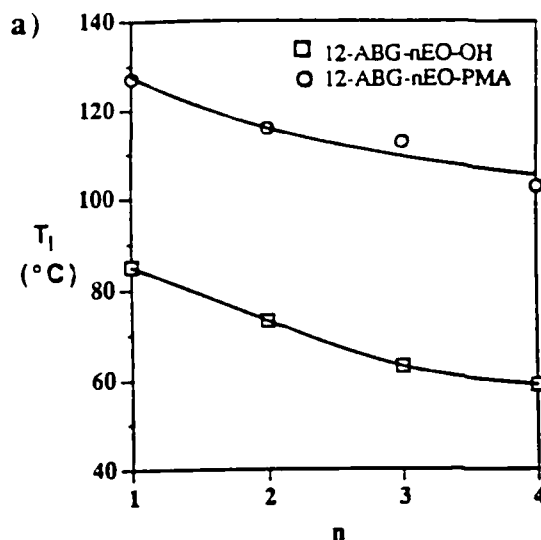
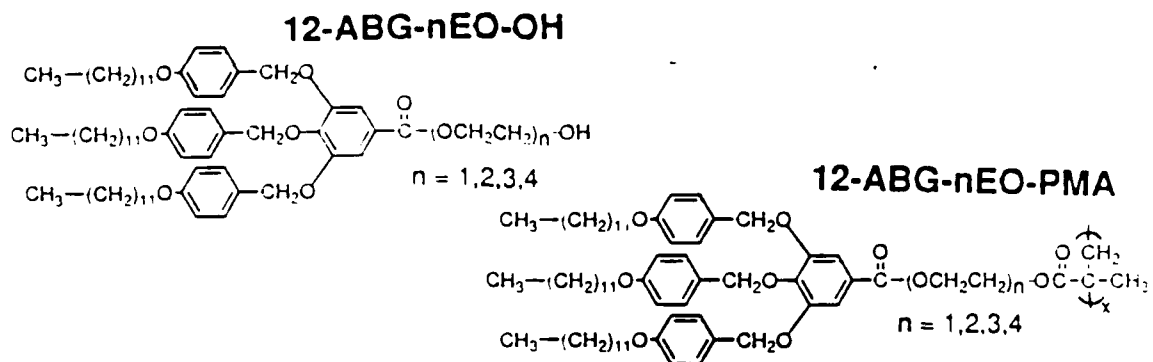
and  $S_{exp}$  determined from the hexagonal lattice parameter are 24.8 Å and 28.5 Å, respectively. The smaller dimensions are expected as a result of the absence of the benzyl ether moieties. The structure of the  $\Phi_h$  mesophase of **12-AG-15C5** is shown in Figure 5d. From these data, it is obvious that the benzyl ether moieties stabilize the  $\Phi_h$  mesophase of the taper shaped structural unit by suppressing crystallization of the alkyl tails and increasing the width of the tapered *exo*-receptor at the column periphery.

Figure 6 shows a comparison of the idealized lowest energy conformation of the cross-section of the  $\Phi_h$  mesophase of **12-ABG-15C5** and the corresponding structure with melted alkyl tails. Similar depictions of **12-ABG-B15C5** and **12-AG-15C5** have been omitted for brevity. In the minimum energy conformation, the alkyl tails are fully extended in an all *trans* configuration. The theoretical radius ( $R_{th}$ ) for the minimum energy conformation was determined by measuring the distance from the center of the column to the outermost alkyl tail of the respective molecular models. In Figure 6,  $R_{th}$  is compared to the experimental radius ( $R_{exp}$ ) determined by x-ray scattering. In each case, a larger value of  $R_{th}$  can be reconciled with the observed radius,  $R_{exp}$ , by shrinkage of the alkyl tails. This shrinkage should be confined to the alkyl tails due to the rigidity of the aromatic internal core of the assembly. The shrinkage is shown in Figure 6 for the three supramolecular assemblies. From the shrinkage, a reasonable estimate of the number of molecules in a column cross-section can be determined. In the case of **12-ABG-B15C5**, six molecules would result in a larger internal core and a correspondingly larger alkyl tail shrinkage of 78%. Additional work in our laboratory has shown alkyl tail shrinkages of 50-60%.<sup>8-10</sup> Therefore, a model composed of five molecules of **12-ABG-15C5** seems more reasonable. In the case of **12-ABG-15C5**, models composed of five and six molecules give acceptable shrinkages of 51% and 57%, respectively. The  $R_{exp}$  of the cross-section of the self-assembled supramolecule derived from **12-ABG-15C5** is ~2 Å larger than the corresponding radius of that derived from **12-ABG-B15C5**. However, the end-to-end distance of the minimum energy conformation of an isolated molecule of **12-ABG-15C5** is ~3 Å shorter than the corresponding dimension of **12-ABG-B15C5**. However, when the supramolecular cylinder of **12-ABG-15C5** is composed of six taper units per column layer instead of five, it would be expected to exhibit a larger  $R_{exp}$ , as is indeed the case.

#### Oligooxyethylene Segments as *Endo*-Receptors: A Comparison Between Supramolecular and Molecular "Polymer Backbones"

**12-ABG-nEO-OH** and **12-ABG-nEO-PMA** shown in Figure 7 self-assemble similarly with the systems based on crown ethers as *endo*-receptor. In this case, the cation selective crown ether *endo*-receptor of the tapered subunit from the previous molecules was replaced with the non-selective oligooxyethylene *endo*-receptor. **12-ABG-nEO-OH** are analogous to **12-ABG-15C5** shown in Figure 4. The value of *n* indicates the number of oligooxyethylene segments and varies from *n* = 1 to 4. **12-ABG-nEO-PMA** are the polymeric analogs of **12-ABG-nEO-OH**. All compounds form an enantiotropic  $\Phi_h$





**Figure 7:** The dependence of  $T_g$  of 12-ABG-nEO-OH (□) and 12-ABG-nEO-PMA (○) versus  $n$  (data from the first DSC heating scans) (a); the dependence of  $R_{exp}$  of 12-ABG-nEO-OH (□) and of 12-ABG-nEO-PMA (○) versus  $n$  (b); a model of the cross-section of the column formed by 12-ABG-3EO-OH (c); a model of the cross-section of the column formed by 12-ABG-3EO-PMA (d).

mesophase which was characterized by a combination of x-ray scattering, thermal optical polarized microscopy, and DSC experiments.<sup>18</sup> The mechanism of formation and stabilization of the self-assembled supramolecular columns is similar for both 12-ABG-nEO-OH and 12-ABG-nEO-PMA but provides access to a systematic investigation of the difference between the two systems as  $n$  is varied.

As  $n$  is increased from 1 to 4 the  $\Phi_h$ -i transition temperatures ( $T_i$ ) for both systems decreases at a similar slope. For all  $n$  presented here,  $T_i$  of 12-ABG-nEO-PMA is consistently about 45°C higher than that of the low molar mass compounds 12-ABG-nEO-OH (Figure 7a). Figure 7b shows the dependence of the experimentally determined column radius ( $R_{exp}$ ) as a function of  $n$ . Increasing  $n$  causes  $R_{exp}$  to increase. The column radii of the polymers are 2 to 4 Å larger than their corresponding monomer compounds 12-ABG-nEO-OH.

Molecular models were constructed for all compounds to provide explanations for these observations in phase behavior and column diameter.<sup>18,19</sup> Figure 7c illustrates a model of a cross-section of the cylinder formed by 12-ABG-nEO-OH with the alkyl tails and the flexible oligooxyethylene spacer melted so that the radius of the model is equivalent to the value determined by x-ray scattering experiments. The oligooxyethylene spacer is confined to the core of the supramolecule as a result of the tapered shape, packing efficiency, and other factors. A more detailed discussion of this system will be presented in the following paragraph and in Figure 9. Figure 7d shows a cross-section of the cylinder formed by 12-ABG-nEO-PMA. The flexible oligooxyethylene spacer in the core of both compounds complexes alkali metal salts. The phase behavior of both systems was characterized as a function of the amount of LiOTf in the complex. Some of these results will be presented in Figure 8. As a result of these experiments, Li cations (represented as filled atoms) are placed in the most likely sites of coordination within the cross-section of the models in Figure 7c and d.

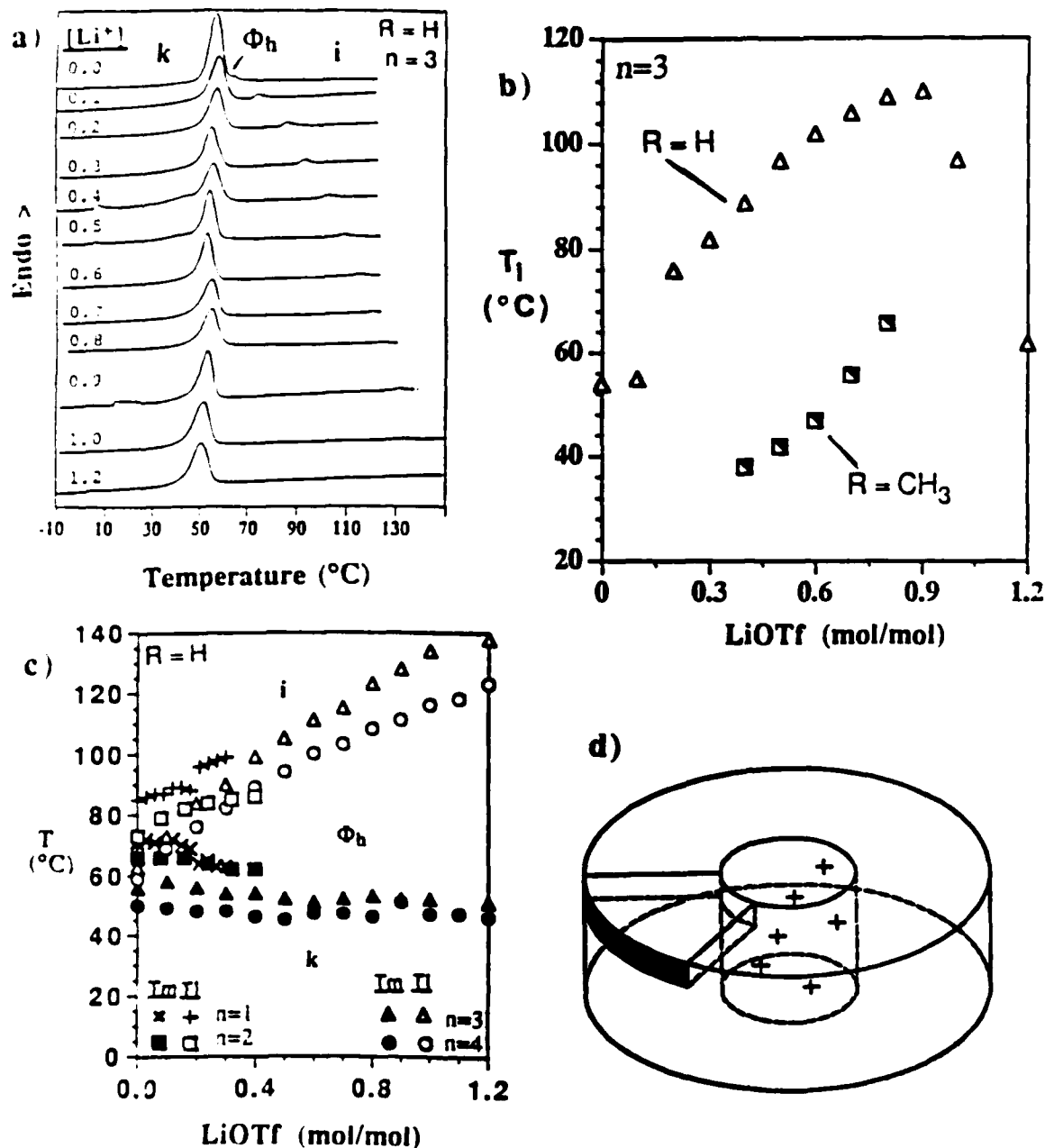
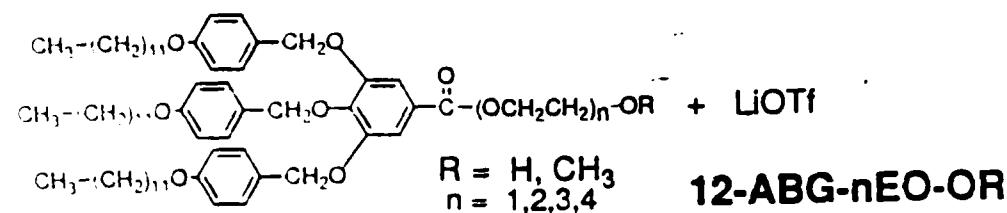
The model of 12-ABG-nEO-OH in Figure 7c demonstrates that the formation of the supramolecular column results from several factors. The tapered and effectively flat shape favors the packing into a cylindrical arrangement as opposed to a lamellar or spherical packing. As a result of the molecular design, the polar  $\omega$ -hydroxyoligooxyethylene segments are concentrated in the core of the assembly. The main forces responsible for this arrangement are hydrogen bonding (H-bonding) and electrostatic attractive interactions of the flexible oligooxyethylene segments as well as microsegregation of these polar groups from the non-polar aliphatic and aromatic groups at the column periphery. When LiOTf is added, the microsegregation and attractive interactions in the core of this assembly are enhanced by the complexation of the salt which provides a thermodynamic stabilization to the self-assembled structure and shifts the  $T_i$  to higher temperatures. The effect of the contribution of the polymer backbone is illustrated with the model in Figure 7d. The linear nature of the polymer backbone imposes restrictions on the placement of the taper shaped side groups within the column that are not present with the low molar mass analogs 12-ABG-nEO-OH

Based on x-ray scattering, density (obtained at 23° C), and an assumed layer thickness of the cross-section (based on a literature value), an approximate of 6 tapered side groups must occupy a cross-section of the column. It is assumed that the column is formed by a single polymer chain. There is not yet any definitive evidence to disprove this assumption. For the necessary amount of side groups to occupy a cross-section of the column, the polymer backbone must adjust its conformation cooperatively.

The self-assembly of **12-ABG-nEO-PMA** can be qualitatively compared with **12-ABG-nEO-OH** with respect to the forces responsible for the self-assembly process. The replacement of the weak H-bonding of the pendent OH groups with the much stronger covalent bond to the polymer backbone provides a greater force holding the taper shaped groups together and increases the thermodynamic stability of the supramolecular structure (see Figure 7a). The disadvantage provided by the covalent attachment to the polymer backbone and the elimination of the pendent OH group is that the non-selective and flexible oligooxyethylene segments are not able to complex as much LiOTf or interact with the salt as efficiently as in the low molar mass compounds **12-ABG-nEO-OH**.

The effect of the LiOTf on the phase behavior of the complex is shown in Figure 8 for the compounds **12-ABG-nEO-OH**<sup>18,19</sup> with  $n = 1$  to 4 and for the model compound **12-ABG-3EO-OCH<sub>3</sub>**.<sup>18</sup> Figure 8a displays representative DSC traces of **12-ABG-3EO-OH** with increasing the amount of LiOTf. The peak associated with the  $T_i$  systematically increases as the amount of LiOTf increases, while the crystalline melting transition ( $k$ ) remains constant. The effect of replacing the OH with a CH<sub>3</sub> group is shown in Figure 8b. The OH group provides stabilization to the self-assembled structure *via* H-bonding. The pendent OCH<sub>3</sub> group can only participate in weak electrostatic attractive interactions and introduces the possibility of repulsive steric interactions in the core of the supramolecular structure as a result of its increased size. Compound **12-ABG-3EO-OCH<sub>3</sub>** which contains an OCH<sub>3</sub> terminal group in the *endo*-receptor exhibits a  $T_i$  about 40°C lower than **12-ABG-3EO-OH** which has an OH terminal group in the *endo*-receptor. Also, **12-ABG-3EO-OCH<sub>3</sub>** is not able to complex as much LiOTf as **12-ABG-3EO-OH**. The last value presented in Figure 8b is 0.8 moles LiOTf per repeat unit. Above this value a crystalline phase appears which may be the result of the formation of LiOTf aggregates. It should be pointed out that amounts of LiOTf larger than 0.8 moles per mole of **12-ABG-3EO-OH** and temperatures higher than 120° C cause Lewis acid catalyzed decomposition of the *p*-alkoxybenzyl ether groups. This produces the downward curvature of the  $T_i$  temperatures on cooling and second heating scans with increasing the amount of LiOTf (Figure 8b).

The dependence of the transition temperature on the length of the oligooxyethylene spacer of **12-ABG-nEO-OH** plotted versus the concentration of complexed LiOTf is shown in Figure 8c. **12-ABG-1EO-OH** and **12-ABG-2EO-OH** have short oligooxyethylene spacers and are able to complex 0.3 moles and 0.4 moles of LiOTf per taper shaped group, respectively. **12-ABG-3EO-OH** and **12-ABG-4EO-OH** have longer oligooxyethylene segments with a larger number of electron rich donor oxygen atoms and are



**Figure 8:** (a) Representative DSC traces of 12-ABG-3EO-OH with increasing concentrations of lithium triflate (LiOTf) per mole of 12-ABG-3EO-OH ([Li<sup>+</sup>]) (first DSC heating scans); (b) the dependence of the T<sub>i</sub> for 12-ABG-3EO-OH (Δ) and 12-ABG-3EO-OCH<sub>3</sub> (◻) versus LiOTf concentration (data from the first DSC cooling scans); (c) the dependence of the T<sub>m</sub> and T<sub>i</sub> versus LiOTf concentration of 12-ABG-nEO-OH for n = 1 (x+), n = 2 (◼◻), n = 3 (▲Δ), and n = 4 (●○) (data from the first DSC heating scans); (d) a representation of the self-assembled cylindrical structure with dissolved salts in the core.

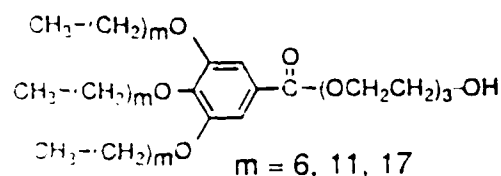
able to complex up to 1.2 moles of LiOTf per taper shaped group. Above this value  $T_i$  values are in the range where decomposition begins to occur. This prevents determination of the upper limit of LiOTf that can be complexed.

It is now possible to make a quantitative comparison of the electrostatic, ionic, and H-bonding (i.e., supramolecular interactions), with molecular "interactions" (generated via a conventional molecular polymer backbone) responsible for generating this supramolecular architecture. It requires interactions in the core provided by 0.7 moles of LiOTf per structural unit for the cylindrically shaped structure formed by **12-ABG-3EO-OCH<sub>3</sub>** to have the same thermodynamic stability that results from the H-bonding of the OH group of **12-ABG-3EO-OH** without complexed LiOTf (see Figure 8b).

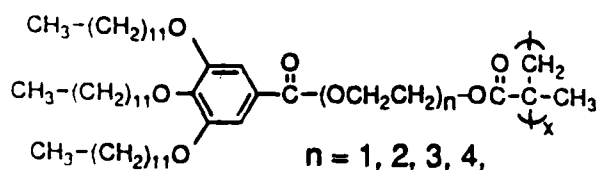
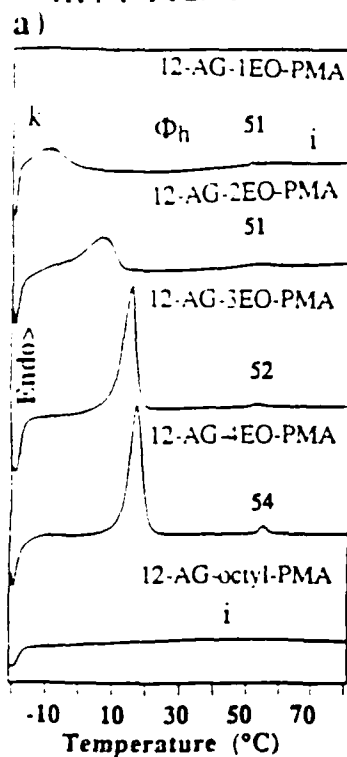
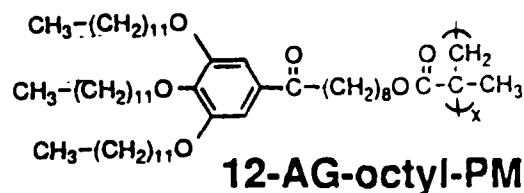
This provides a measure of the contribution of H-bonding to the self-assembly of the supramolecular cylinders. A direct comparison of the effect of a non-covalent (supramolecular) polymer backbone and a covalent (molecular) polymer backbone can be made by comparing **12-ABG-3EO-OH** and **12-ABG-3EO-PMA**. **12-ABG-3EO-OH** requires 0.65 moles of LiOTf per structural unit in conjunction with the H-bonding present to equal the same thermodynamic stability of the cylinder that is generated by the polymethacrylate backbone (i.e., 45° C higher  $T_i$ , see Figure 7a and 8c). In addition to providing a direct comparison between *molecular* and *supramolecular* "polymer effects", these observations further highlight the structural tools that can be used to regulate the internal interactions of these tubular structures.

A representation of the self-assembled cylindrical supramolecular structure formed by these compounds is shown in Figure 8d.<sup>19</sup> Cations (represented as the +s) are placed in the core of this cylinder where the flexible oligooxyethylene segments reside. Questions remain about the location of the anions or about the possibility that the alkyl-phenyl and benzyl-phenyl ether oxygen atoms contribute to the complexation of high amounts of Li cations.

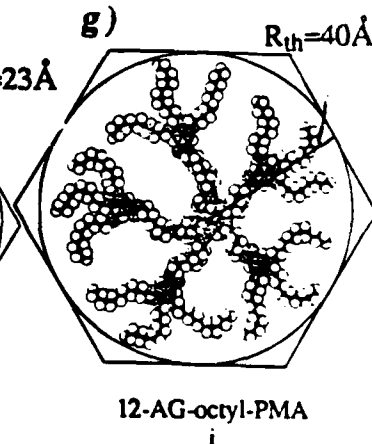
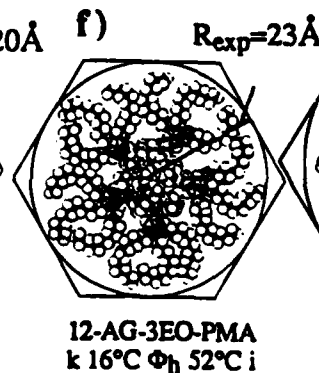
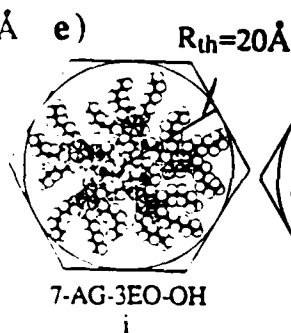
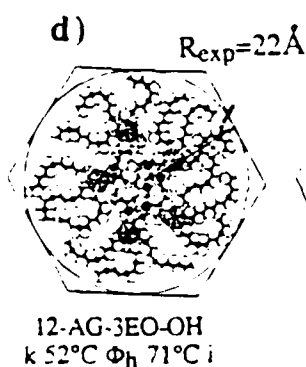
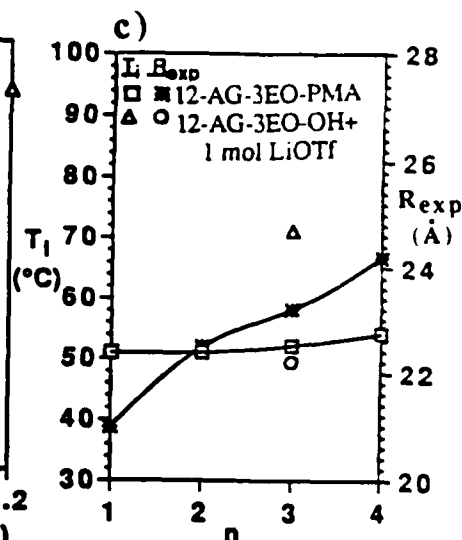
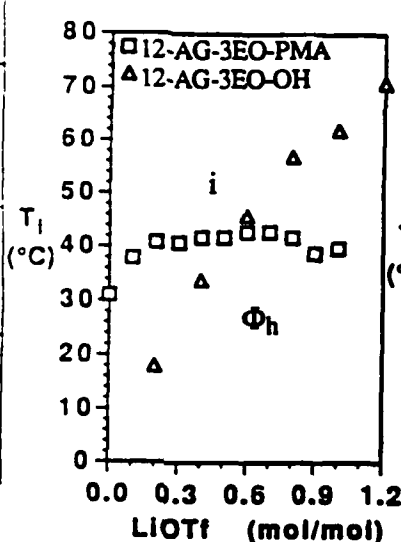
The main forces responsible for the self-assembly process that have been presented so far are dramatically illustrated with **m+1-AG-3EO-OH** and **12-AG-nEO-PMA** shown in Figure 9.<sup>20</sup> These compounds are of similar design to **12-ABG-nEO-OH** and **12-ABG-nEO-PMA** which are shown in Figure 7, with the exception that the 3 benzyl ether groups from the *exo*-receptor are absent. This change decreases  $T_i$  with approximately 50-70°C for most of the compounds and allows the demonstration of the critical *exo*-molecular recognition interactions present in these systems. **12-AG-octyl-PMA**<sup>20</sup> is a model compound for **12-AG-3EO-PMA** and has an octyl spacer connecting the tapered side group to the polymethacrylate backbone. Replacement of the triethyleneoxide spacer with an n-octyl spacer having the same number of atoms removes the electrostatic attractive interactions present in the core resulting from EO spacer, provides a slight increase in the rigidity of the spacer, and as a result of its hydrophobic character it reduces the stabilization provided to the assembly *via* microsegregation of hydrophilic and hydrophobic functionalities. The DSC traces of **12-AG-nEO-PMA** with  $n = 1$  to 4 and of **12-AG-octyl-PMA** are shown in Figure 9a. All **12-AG-nEO-PMA** display an enantiotropic  $\Phi_h$  mesophase with  $T_i$  between



**m+1-AG-3EO-OH**



b) **12-AG-nEO-PMA**



**Figure 9:** (a) Representative DSC traces of 12-AG-nEO-PMA for  $n=1$  to 4 and of 12-AG-octyl-PMA (first DSC heating scans); (b) the dependence of the  $T_g$  for 12-AG-3EO-PMA ( $\square$ ) and 12-AG-3EO-OH ( $\Delta$ ) versus lithium triflate (LiOTf) concentration (data from the first DSC cooling scans); (c) the dependence of the  $T_g$  versus  $n$  (data from the first DSC heating scans) on the left y-axis and the dependence of the column radius determined from x-ray scattering experiments on the right y-axis for 12-AG-nEO-PMA ( $\square$ ) and 12-AG-3EO-OH with 1.0 moles of complexed LiOTf ( $\Delta$ ); and molecular model cross-sections of the cylindrically shaped structures of: (d) 12-AG-3EO-OH; (e) 7-AG-3EO-OH; (f) 12-AG-3EO-PMA; (g) 12-AG-octyl-PMA

51° and 54°C, as well as a crystalline (k) melting transition. **12-AG-octyl-PMA** is only liquid within the temperature range examined. The changes that result from replacing the EO spacer with a paraffinic spacer destroy its ability to form both k and  $\Phi_h$  phases.

A direct comparison of the self-assembly of the low molar mass **12-AG-3EO-OH** by only non-covalent interactions, and the self-assembly that occurs as a result of covalent attachment to a polymethacrylate backbone in conjunction with non-covalent interactions (**12-AG-3EO-PMA**) is outlined in Figure 9b.  $T_i$  is plotted versus the amount of LiOTf present in the complex. Initially, the polymer backbone provides a greater thermodynamic stability to the self-assembled structure. At the LiOTf molar ratio of 0.6, the polymer and the low molar mass compounds have approximately equivalent  $T_i$  values. As the amount of LiOTf is further increased, the  $T_i$  of **12-AG-3EO-OH** continues to increase, whereas the  $T_i$  of **12-AG-3EO-PMA** does not. The non-covalently bound **12-AG-3EO-OH** is able to adjust its position and conformation within the column to take advantage of enhanced interactions in the core that result from the complexed salt. Although the polymer backbone initially provides a greater thermodynamic stability to the supramolecular architecture by causing positional restrictions, at higher salt ratios these positional restrictions hinder the tapered side groups from benefiting from the interaction resulting from the complexed LiOTf.

Molecular models of some of these compounds are presented in Figure 9d-g. **12-AG-3EO-OH** is shown in Figure 9d. It forms a  $\Phi_h$  mesophase upon the addition of LiOTf. **7-AG-3EO-OH** which has shortened alkyl tails is outlined in Figure 9e. The latter does not form a  $\Phi_h$  mesophase upon the complexation of LiOTf. It can be observed from the models in Figure 9d and e that the short alkyl tails of **7-AG-3EO-OH** are not sufficiently efficient to provide a hydrophobic barrier around the polar  $\omega$ -hydroxyoligooxyethylene segments. A model of **18-AG-3EO-OH** is not shown in Figure 9 which has alkyl tails with six methylenic units longer than **12-AG-3EO-OH**. It also forms a  $\Phi_h$  mesophase, but has higher  $T_i$  than **12-AG-3EO-OH** at the same ratios of LiOTf.<sup>20</sup> The increase in  $T_i$  for **18-AG-3EO-OH** is attributed to the longer alkyl tails which provide a greater hydrophobic contribution to the microsegregation and thus stabilizes the cylindrically shaped assembly. Models of **12-AG-3EO-PMA** and **12-AG-octyl-PMA** are shown in Figure 9f and g, respectively. The electrostatic attractive interactions that result from the oligooxyethylene spacer in **12-AG-3EO-PMA** (Figure 9f) are absent in the paraffinic spacer of **12-AG-octyl-PMA** (Figure 9g) and cannot hold the tapered side groups in a close arrangement around the polymer backbone.

Compounds **m+1-AG-nEO-OH** and **12-AG-nEO-PMA** represent a self-assembled supramolecular system in which the molecular recognition interactions are delicately balanced. Structural changes which affect these interactions produce dramatic changes in the diameter and flexibility of the self-assembled cylinders and subsequently in the thermodynamic stability of the  $\Phi_h$  mesophase resulting from them.

### Endo-Receptors Based on H-bonding

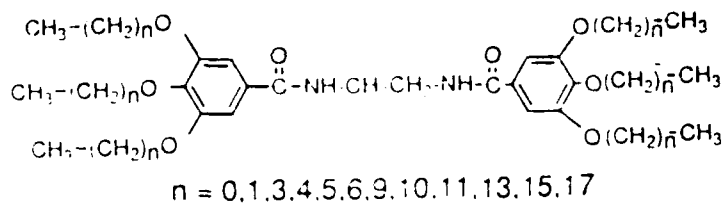
Compounds **n+1-AG-DA2**, which are shown on the top of Figure 10, form cylindrically shaped supramolecules by somewhat different interactions and molecular packing principles than the previous systems presented in this paper.

**n+1-AG-DA2** have two taper shaped groups connected at the 1 and 2 positions of an ethylenic spacer by benzamido functionalities. They form a  $\Phi_h$  mesophase, depending on the tail length, as a result of H-bonding.<sup>21</sup> **n+1-AG-DA2** can form these H-bonds between the NH hydrogen donor (H-donor) and C=O hydrogen acceptor (H-acceptor) groups. A more detailed discussion of a possible H-bonding motif within the columns will be presented in Figure 11. **12-AG-DE2** was synthesized as a model compound for **12-AG-DA2** since it has the same molecular structure with the exception that the NH groups have been replaced with an ester O atom. For **12-AG-DE2** the C=O groups are capable of forming H-bonds with a H-donor group. The replacement of the NH group by an O, eliminates the H-donor group from the molecule. Consequently, **12-AG-DA2** (also all **n+1-AG-DA2**) in the bulk form can form H-bonds, whereas **12-AG-DE2** cannot, unless a second component bearing a H-donor group is added. DSC scans of pure **12-AG-DA2** and **12-AG-DE2** are shown in Figure 10a. Both compounds have similar structures so it is not surprising that they exhibit identical melting temperatures on the first DSC heating scan ( $T_m = 63^\circ\text{C}$ ). As a result of **12-AG-DA2**'s functional capability to self-H-bond in bulk form, it maintains a  $\Phi_h$  mesophase up to  $129^\circ\text{C}$ . **12-AG-DE2**, which cannot self-H-bond, melts from a crystalline phase (k) directly into an isotropic liquid (i). The self-H-bonding is one of the essential factors required by these molecules to form a cylindrically shaped assembly which generates a  $\Phi_h$  mesophase.

Another critical factor is the length of the alkyl tails. Figure 10b shows the phase behavior of **n+1-AG-DA2** determined by x-ray scattering, thermal optical polarized microscopy, and DSC experiments as a function of the alkyl tail length (n+1).<sup>21</sup> **n+1-AG-DA2** with alkyl tail lengths  $\geq 10$  methylenic units display a  $\Phi_h$  mesophase. When the alkyl tail length is  $\leq 7$  methylenic units, these compounds exhibit only crystalline phases. For **n+1-AG-DA2** with n=3, 4, 5, and 6 the uppermost phase is identified as a distorted crystalline hexagonal phase ( $k_{dhex}$ ). **5-AG-DA2** displays a truly hexagonal crystalline phase ( $k_{hex}$ ) at room temperature. In Figure 10c, extrapolation of the experimentally determined column diameters ( $a_n$ ) in the  $\Phi_h$  and  $k_{hex}$  phases to an alkyl chain length of 0 methylenes gives a rigid core diameter ( $a_0$ ) of 15.2 Å (refer to Figure 10d for illustrative definitions of  $a_n$  and  $a_0$ ). This value is used to construct molecular models as an approximate of the core diameter.

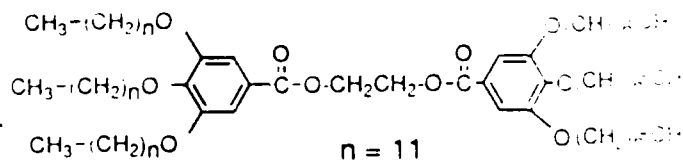
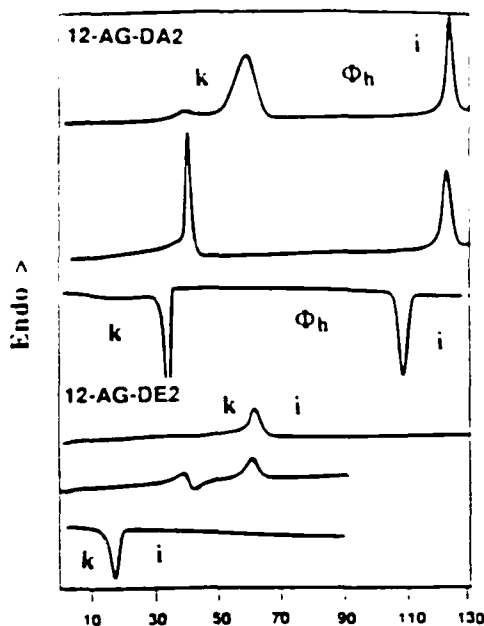
Based on these experimental results, we have been able to construct an estimated model of the molecular packing and H-bonding contacts within the column. In formulating this model we have taken into account the experimentally determined column diameters, the extrapolated core diameter, a representative density measurement for **12-AG-DA2** (obtained at  $23^\circ\text{C}$ ), optimum H-bonding distances and angles for amides, additional attractive and





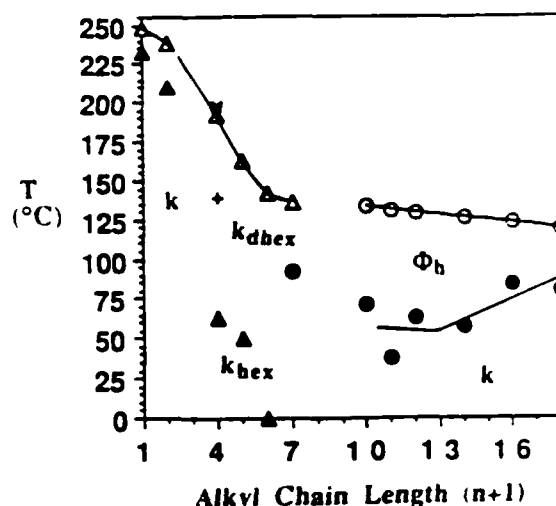
### n+1-AG-DA2

a)

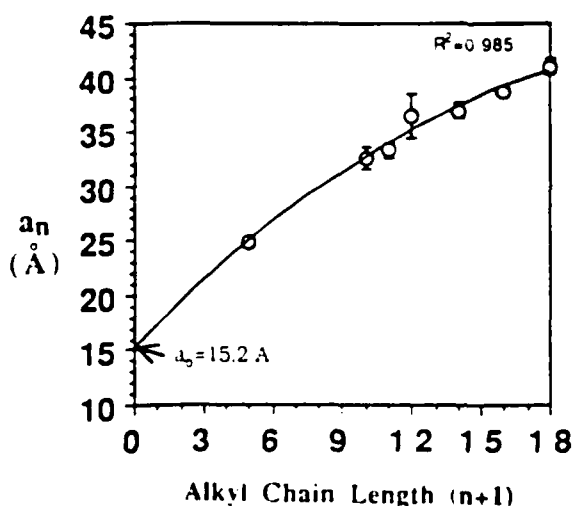


### 12-AG-DE2

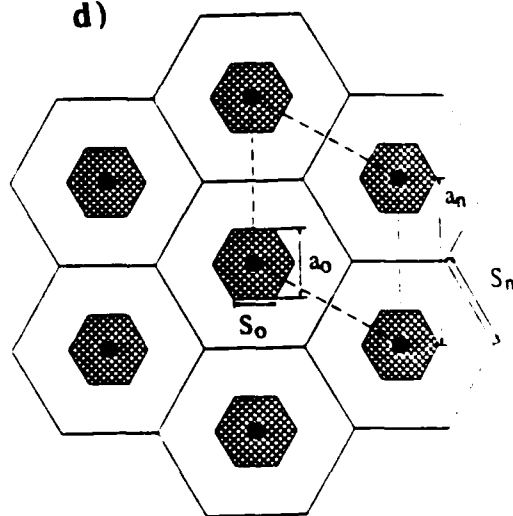
b)



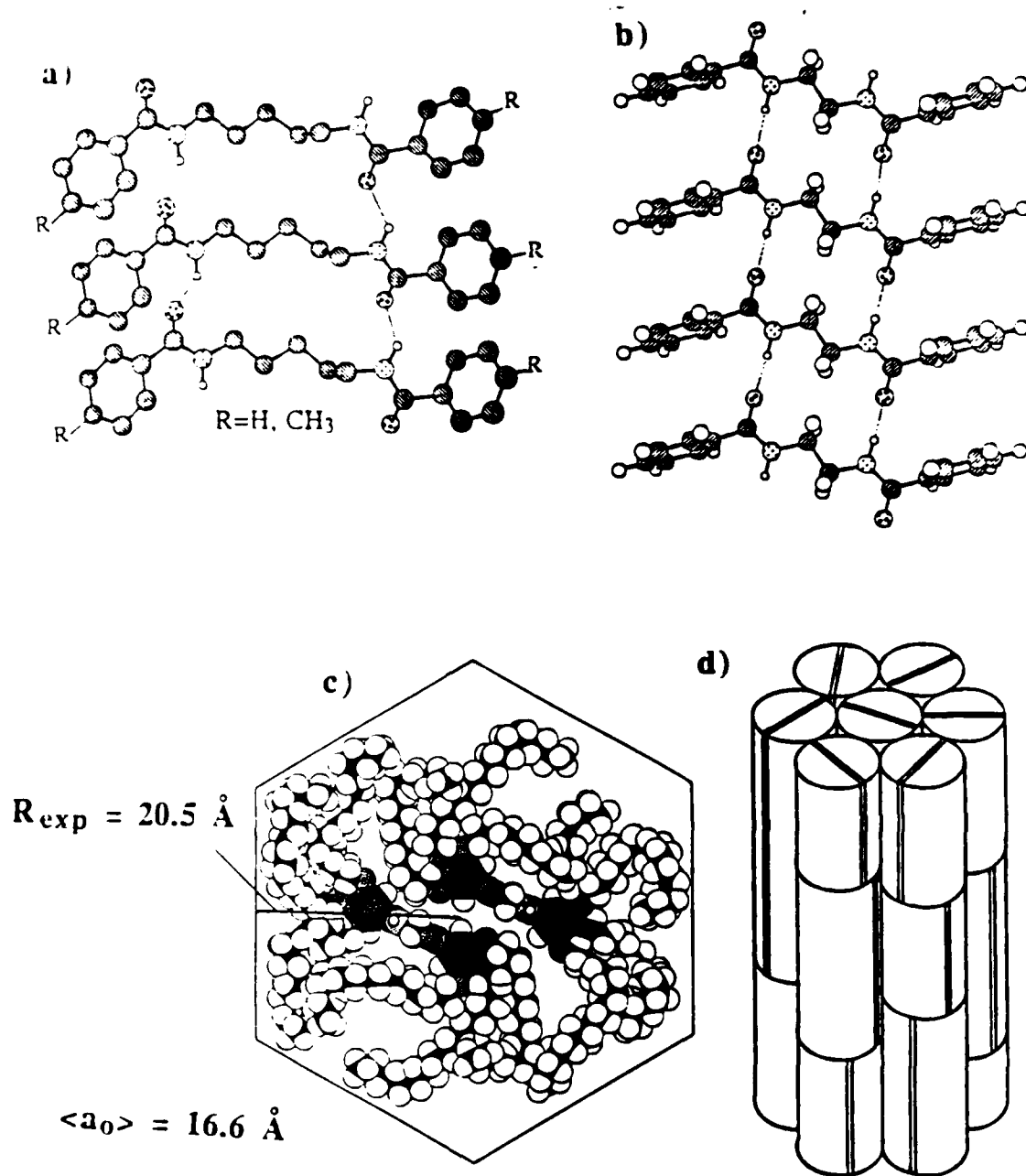
c) Temperature (°C)



d)



**Figure 10:** (a) DSC traces from the first heating scan, second heating scan, and first cooling scan (top to bottom) for 12-AG-DA2 and 12-AG-DE2; (b) the phase behavior of n+1-AG-DA2 versus alkyl tail length (n+1); (c) extrapolation of the experimentally measured column radius ( $a_n$ ) determined from x-ray scattering experiments in the  $k_{\text{hex}}$  of  $\Phi_h$  phases versus alkyl tail length; (d) illustrative definitions of  $a_n$ ,  $a_0$ ,  $S_n$ , and  $S_0$  for the hexagonal columnar phase.



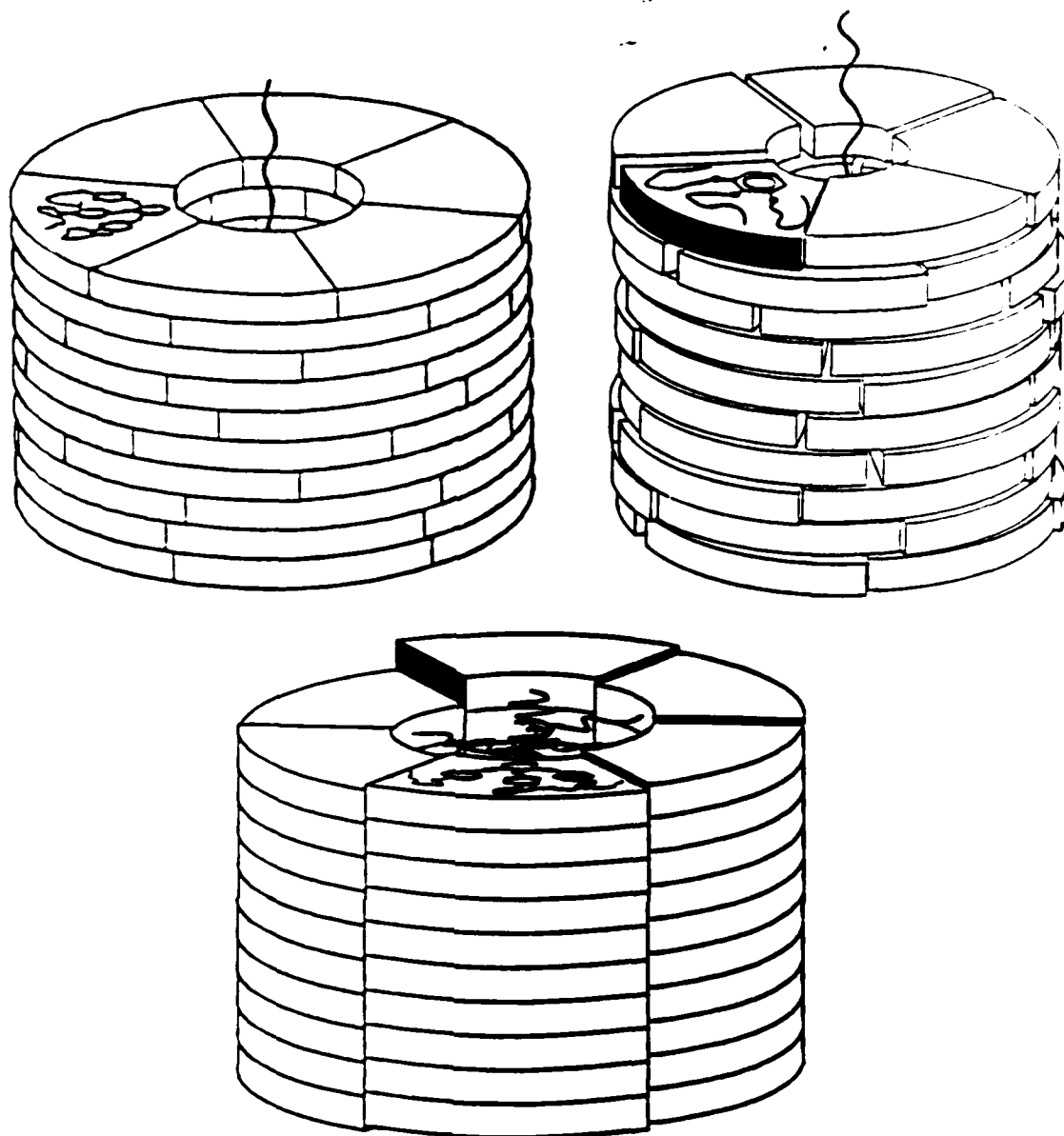
**Figure 11:** (a) Pleated ribbon packing of molecules of related bisamides in the crystal structure; (b) a side view of the proposed H-bonding in the  $\Phi_h$  mesophase of  $n+1$ -AG-DA2 (for  $n+1 \geq 10$ ) along the column axis; (c) a top view of a cross-section of the column formed by 18-AG-DA2 with alkyl tails melted; (d) a representation of 2 columns (semicolumns) of  $n+1$ -AG-DA2 forming a column which packs into the hexagonal lattice of the  $\Phi_h$  mesophase.

repulsive Van der Waals interactions, and the possibility of intramolecular H-bonds versus intermolecular H-bonds. Also, the packing of related bisamides shown in Figure 11a obtained from their crystal structure was taken into consideration. The most likely model of the column core which can explain all results is shown in Figure 10b. This is a side view of the column formed by  $n+1$ -AG-DA2 with  $n \geq 9$ . H-bonding occurs intermolecularly vertically along the column axis. The ethyl spacer is in a low energy trans conformation. The aromatic rings are shown relatively perpendicular to the column axis. It is possible that they are tilted or oscillate when in the  $\Phi_h$  phase. This H-bonding motif results in a net translation which would produce a tilted column. To offset this we have tilted the molecules along the column axis.

Figure 11c shows the top view of a cross-section of the column formed by this packing. The alkyl tails have been added and melted above and below the plane of the cross-section. Apparent areas of void would be filled by the melted alkyl tails from cross-sections above and below this cross-section. In order to meet the requirements of the results obtained from x-ray scattering and density measurements, the column must be composed of two independent columns (semicolumns) which are H-bonded along the column axis and pressed against each other in the middle. Although there may exist some attractive or repulsive interactions at the interface between the two semi-columns (see the apparent lock-and-key generated at the interface), the principal forces that lead to this type of packing arrangement would be the tetra coordinate H-bonding of the molecules along the column axis and the packing efficiency of the melted alkyl tails surrounding the rigid aromatic cores.

Careful observation of the aromatic core of this model reveals that it has an elliptical shape rather than a circular one. This provides a possible explanation for the phase behavior presented in Figure 10b. With long alkyl tails ( $n+1 \geq 10$ ) the melted alkyl periphery may average to a circular shape within a cross-section of the column thereby producing a symmetrical cylinder. But for shorter alkyl tails ( $n+1 \leq 7$ ) this averaging may not be able to produce a circular shaped periphery as a result of the molecular placement in the core. Without a circular shape, the columns cannot pack into a regular hexagonal lattice. The net result would be a distorted hexagonal lattice and indeed a distorted hexagonal phase ( $k_{dhex}$ ) is observed. Lack of sufficient melted alkyl content can explain the change from a liquid crystalline phase to a crystalline phase that occurs with this decrease in alkyl tail length. A minimum amount of disordered alkyl chains between the columns is needed to disrupt the registry of the layers between the columns and produce a liquid crystalline phase as opposed to a crystalline phase. Decreasing the alkyl tails from ten to seven methylenic units falls below this minimum amount.

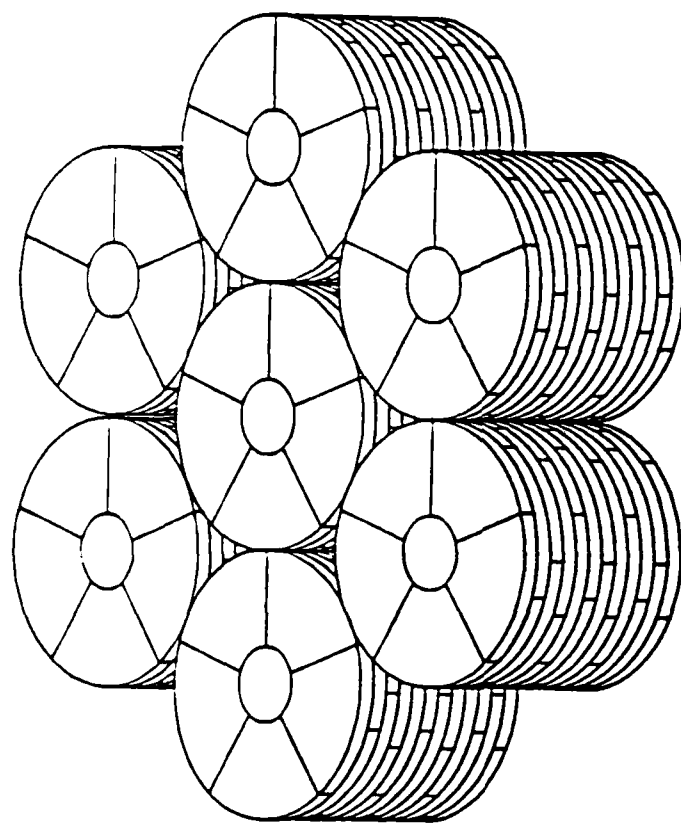
Figures 11d and 12 illustrate the proposed different mechanisms of the self-assembly of cylindrically shaped tubular supramolecular architectures presented in this paper.<sup>18,20,22</sup> Figure 11d illustrates the semicolumns of  $n+1$ -AG-DA2 which form cylinders that pack into a hexagonal lattice generating a  $\Phi_h$  mesophase. Figure 12 shows different representations of what the spontaneous packing of the side groups might possibly be for the



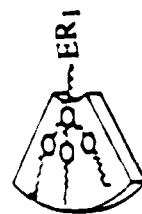
**Figure 12:** Different possibilities of the **packing of the tapered side groups** of the polymers that form tubular supramolecular architectures.

polymers (and monomers) which form the **tubular supramolecular architectures** presented here. Possibly they may pack tightly or loosely to form **disk-like substructures** which pack into a column. Or there may be a kind of **helical packing** that results from the linear nature of the polymer backbone. Additionally, there is also the possibility that two or more polymer chains cooperatively form a column.

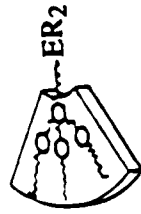
The different approaches used to generate tubular supramolecular architectures are summarized in Figure 13. With these structural and functional changes, the  $T_i$  of these  $\Phi_h$  phases generated from the supramolecular cylinders have been controlled within the temperature range of 7° to 148° C, while the measured column diameters varied in the range of 42 to 61 Å as expected based on the dimensions of the individual molecular subunits. As presented in detail elsewhere,<sup>22</sup> the tapered shaped subunits bearing different functional groups



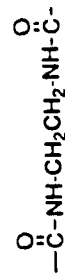
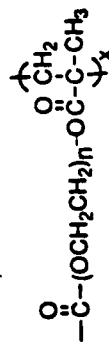
**Figure 13:** Summary of the different *endo*-receptors used to generate tubular supramolecular assemblies and the co-assembly of the taper shaped groups that have different *endo*-receptors into a single cylinder.



+



ER<sub>1</sub> or ER<sub>2</sub>



-CE

can co-assemble cooperatively to form similar structures subject to the limitations resulting from spatial packing as well as the thermodynamic and kinetic factors of the recognition processes. For example, the tapered groups with different length of the  $\omega$ -hydroxyoligooxyethylene groups co-assemble over the entire range of compositions. However, the tapered groups with similar length of the oligooxyethylenic *endo*-receptor but terminated by a pendent OH and a covalent polymer backbone co-assemble only within a limited range of composition. This co-assembly process is considerably enhanced *via* complexation with alkali-metal salts. On the other hand, the tapered groups with  $\omega$ -hydroxyoligooxyethylene and crown ether *endo*-receptors do not co-assemble in the presence of NaOTf but rather self-assemble into independent columns composed of only one kind of tapered subunit as a result of their considerably different strengths and rates of self-assembly versus co-assembly *via* complexation with salts.

The supramolecular cylindrical architectures outlined in Figure 13 provide an entry into the molecular recognition directed self-assembly *via* principles which resemble those of the self-assembly of TMV. So far we can tailor-make the external diameter of these cylinders only within a very limited range. The same can be stated about the diameter of the channel penetrating through these architectures. These supramolecular cylinders self-assemble not only in melt phase but also in solution. The surface of these cylinders can be tailor-made by chemical modification reactions performed on the outer edge of the *exo*-receptors. This work is only at the very beginning and a large variety of structural and dynamic investigations should be performed before a comprehensive understanding of these systems will become available. Nevertheless, even at this stage we foresee a series of new concepts which will emerge from these supramolecular channel-like architectures. For example, preliminary investigations have suggested that they act like supramolecular ionic channels.<sup>11</sup> In these channels, the ionic conductivity is absent in the crystalline phase and takes place in the  $\Phi_h$  and isotropic phases. Electronic channels can be designed *via* similar principles. The contents of these channels can be released *via* external regulation either by the use of temperature or solvent. Chemical reactions can be performed on the ion pairs complexed within the channel and this can open new avenues for nanostructures and catalysis. Polymerization reactions performed within the channels of these supramolecular architectures can generate information about reactions in restricted geometries.

#### ACKNOWLEDGMENTS

Financial support by the National Science Foundation (DMR-92-06781), the Office of Naval Research, and NATO (traveling grant) are gratefully acknowledged.

#### REFERENCES

1. J. M. Lehn, *Angew. Chem. Int. Ed. Engl.*, **27**, 89(1988); (b) D. J. Cram, *Angew. Chem. Int. Ed. Engl.*, **27**, 1009(1988); (c) C. J. Pedersen, *Angew. Chem. Int. Ed. Engl.*, **27**, 1021(1988).

2. (a) J. M. Lehn, *Angew. Chem. Int. Ed. Engl.*, **29**, 1304(1990); (b) H. J. Schneider, *Angew. Chem. Int. Ed. Engl.*, **30**, 1417(1991).
3. For some brief reviews on self-assembly see: (a) J. S. Lindsey, *New J. Chem.*, **15**, 153(1991); (b) G. M. Whitesides, J. P. Matthias, and C. T. Seto, *Science*, **254**, 1312(1991); (c) H. J. Schneider and H. Durr, Eds., *Frontiers in Supramolecular Organic Chemistry and Photochemistry*, VCH, New York, 1991; (d) J. M. Lehn, *Makromol. Chem., Macromol. Symp.*, **69**, 1(1993).
4. (a) J. Rebek, Jr., *Angew. Chem. Int. Ed. Engl.*, **29**, 245(1990); (b) D. Philp and J. F. Stoddart, *Synlett*, 445(1991).
5. A. Klug, *Angew. Chem. Int. Ed. Engl.*, **22**, 565(1983).
6. J. N. Israelachvili, *Intermolecular and Surface Forces*, Academic Press, New York, 1992, p. 380.
7. (a) G. H. Brown and J. J. Wolken, *Liquid Crystals and Biological Structures*, Academic Press, New York, 1979, p. 35; (b) V. Degiorgio and M. Corti, Eds., *Physics of Amphiphiles: Micelles, Vesicles, and Microemulsions*, North-Holland, New York, 1985, p.7.
8. V. Percec, J. Heck, and G. Ungar, *Macromolecules*, **24**, 4597(1991).
9. V. Percec, M. Lee, J. Heck, H. E. Blackwell, G. Ungar, and A. Alvarez-Castillo, *J. Mater. Chem.*, **2**, 931(1992).
10. V. Percec, M. Lee, J. Heck, G. Ungar, and A. Alvarez-Castillo, *J. Mater. Chem.*, **2**, 1033(1992).
11. V. Percec, G. Johansson, J. Heck, G. Ungar, and S. V. Batty, *J. Chem. Soc. Perkin Trans. 1*, 1411(1993).
12. G. Johansson, V. Percec, G. Ungar, and D. Abramic, *J. Chem. Soc. Perkin Trans. 1*, in press.
13. D. M. Dishong, C. J. Diamond, M. I. Cinoman, and G. W. Gokel, *J. Am. Chem. Soc.*, **105**, 586(1983).
14. K. Kikukawa, G. X. He, A. Abe, T. Goto, R. Arata, T. Ikeda, F. Wada, and T. Matsuda, *J. Chem. Soc. Perkin Trans. 2*, 135(1987).
15. Y. Takeda, *Top. Curr. Chem.*, **121**, 1(1984).
16. (a) M. A. Bush and M. R. Truter, *J. Chem. Soc. Perkin Trans. 2*, 341(1972); (b) R. Mallinson and M. R. Truter, *J. Chem. Soc. Perkin Trans. 2*, 341, 1818(1972).
17. D. J. Cram, *Angew. Chem. Int. Ed. Engl.*, **25**, 1039 (1986).
18. V. Percec, J. Heck, D. Tomazos, F. Falkenberg, H. Blackwell, and G. Ungar, *J. Chem. Soc. Perkin Trans. 1*, in press.
19. V. Percec, J. Heck, D. Tomazos, and G. Ungar, *J. Chem. Soc. Perkin Trans. 2*, in press.
20. V. Percec, D. Tomazos, J. Heck, H. Blackwell, and G. Ungar, *J. Chem. Soc. Perkin Trans. 2*, in press.
21. V. Percec, J. Heck, G. Ungar, and D. Abramic, to be published.
22. D. Tomazos, G. Out, J. Heck, G. Johansson, V. Percec, and M. Möller, *Liq. Cryst.*, in press.